Fizika Nizkikh Temperatur, 1999, v. 25, No 6, p. 527–550

Magneto-optical spectroscopy of *d*- and *f*-ferromagnetic materials: recent theoretical progress

(Review Article)

V. N. Antonov, A. N. Yaresko, A. Ya. Perlov, and V. V. Nemoshkalenko

Institute of Metal Physics, 36 Vernadsky Street, 252142 Kiev, Ukraine

P. M. Oppeneer and H. Eschrig

Institute of Theoretical Physics, University of Technology, D-01062 Dresden, Germany

Received January 18, 1999

The current status of theoretical understanding of the optical and magneto-optical (MO) spectra of $3d$, $4f$ and $5f$ compounds is reviewed. Energy band theory based upon the local spin-density approximation (LSDA) describes the optical and MO spectra of transition metal compounds reasonably well. Examples which we examine in detail are XPt_3 compounds (with $X = 3d$ V, Cr, Mn, Fe, and Co) in the $AuCu_3$ structure, ternary Heusler alloys NiMnSb, PdMnSb, PtMnSb, and MnBi compound. The LSDA, which is capable of describing the spectra of transition-metal alloys with high accuracy, does not suffice for lanthanide compounds having a correlated $4f$ shell. A satisfactory description of the optical spectra could be obtained by using a generalization of the LSDA, in which explicitly f electron Coulomb correlations are taken into account (LSDA+U approach). As examples of this group we consider CeSb and CeBi. For CeSb a record Kerr angle of 90° was very recently reported, 90° is the absolute maximum value that can be measured. It is two orders of magnitude larger than the values that are commonly measured for transition-metal compounds, and about one order of magnitude larger than values maximally achieved for other lanthanide and actinide compounds. A third group consist of uranium $5f$ compounds. In those compounds where the $5f$ electrons are rather delocalized, the LSDA describes the MO spectra reasonably well. As examples of this group we consider UAsSe and URhAl. Particular difficulties occur for the uranium compounds where the $5f$ electrons are neither delocalized nor localized, but more or less semilocalized. Typical examples are US, USe and UTe. The semilocalized $5f$'s are, however, not inert, but their interaction with conduction electrons plays an important role. Recently achieved improvements for describing such compounds are discussed.

PACS: **71.28.+d**, 71.25.Pi, 75.30.Mb

Contents

© V. N. Antonov, A. N. Yaresko, A. Ya. Perlov, V. V. Nemoshkalenko, P. M. Oppeneer, and H. Eschrig, 1999

Introduction

It was first observed in 1877 by J. Kerr [1] that when linearly polarized light is reflected from a magnetic solid, its polarization plane becomes rotated over a small angle with respect to that of the incident light. This discovery has become known as the magneto-optical (MO) Kerr effect. The Kerr effect is closely related to other anomalous spectroscopic effects, like the Faraday effect and the circular dichroism. These effects all have in common that they are due to a different interaction of left- and right-hand circularly polarized light with a magnetic solid. The Kerr effect has now been known for more than a century, but it was only in recent times that it became the subject of intensive investigations. The reason for this recent development twofold: first, the Kerr effect gained considerable interest due to modern data storage technology, because it can be used to «read» suitably stored magnetic information in an optical manner [2] and second, the Kerr effect has rapidly developed into an appealing spectroscopic tool in materials research. The technological research on the Kerr effect was initially motivated by the search for good magneto-optical materials that could be used as information storage medium. In the sequence of this research, the Kerr spectra of many ferromagnetic materials were investigated. Over the years the Kerr spectra of many ferromagnetic materials have been investigated. An overview of the experimental data collected on the Kerr effect can be found in the review articles by Buschow [3], Reim and Schoenes [4], and Schoenes [5]. The quantum mechanical understanding of the Kerr effect began as early as 1932 when Hulme [6] proposed that the Kerr effect could be attributed to spin-orbit (SO) coupling (see, also Kittel [7]). The symmetry between left- and right-hand circularly polarized light is broken due to the SO coupling in a magnetic solid. This leads to different refractive indices for the two kinds of circularly polarized light, so that incident linearly polarized light is reflected with elliptical polarization, and the major elliptical axis is rotated by the so called Kerr angle from the original axis of linear polarization. The first systematic study of the frequency dependent Kerr and Faraday effects was developed by Argyres [8] and later Cooper presented a more general theory using some simplifying assumptions [9]. The very powerful linear response techniques of Kubo [11] gave general formulas for the conductivity tensor which are being widely used now. A general theory of frequency dependent conductivity of ferromagnetic (FM) metals over a wide range of frequencies and temperatures was developed in 1968 by Kondorsky and Vediaev [12].

The main problem afterward was the evaluation of the complicated formulas involving MO matrix elements using electronic states of the real FM system. With the tremendous increases in computational power and the concomitant progress in electronic structure methods the calculation of such matrix elements became possible, if not routine. Subsequently many earlier, simplified calculations have been shown to be inadequate, and only calculations from «first-principles» have provided, on the whole, a satisfactory description of the experimental results [13]. The existing difficulties stem either from problems using the local spin density approximation (LDA) to describe the electronic structure of FM materials containing highly correlated electrons, or simply from the difficulty of dealing with very complex crystal structures. For 15 years after the work of Wang and Callaway [13] there was a lull in MO calculations until MO effects were found to be important for magnetic recording and the computational resources had advanced. Different reliable numerical schemes for the calculation of optical matrix elements and the integration over the Brillouin zone have been implemented, giving essentially identical results [14]. Prototype studies have been performed using modern methods of band theory for Fe, Co and Ni. Following the calculations for the elemental $3d$ ferromagnets, a number of groups have evaluated the MO spectra for more interesting compounds [15–33] and multilayers [34-40]. While the calculations showed there is good agreement between theory and experiment in case of d-band magnetic materials, attempts to describe MO properties of materials using the same formalism failed to create a consistent physical picture. This has been attributed to the general failure of the LDA in describing the electronic structure of f-state materials ($4f$ especially). To overcome the LDA limitations to study MO spectra a so called E^3 correction for correlations was implemented but gave inconsistent results [30]. The more consistent LDA+U scheme has been used to describe the Kerr angle of CeSb [31,32]. Since then several papers implementing the LDA+U scheme for MO calculations have been published with for $4f$- and $5f$-materials [20,28,30,32,33].

With the above as background, we have performed calculations to evaluate the MO properties for a number of $3d$, $4f$, and $5f$ FM materials. Besides the inherent interest in the materials studied, the use of similar methods to study materials with different degrees of localized electronic states

helps to establish the limitations of the LDA approach and to identify where techniques like the LDA+U method are needed.

The paper is organized as follows. The theoretical framework is explained in Sec. 1. Section 2 presents the electronic structure and MO spectra of $3d$ transition metal compounds XPt_3 (X = V, Cr, Mn, Fe and Co), Heusler alloys (NiMnSb, PdMnSb and PtMnSb) and MnBi compound calculated in the LDA. Section 3 devoted to MO properties and electronic structure of $4f$ compounds (CeSb and CeBi) calculated in LDA and LDA+U approximations. Section 4 considers uranium compounds UAsSe, URhA1, US, USe and UTe. Finally, we present a Summary.

1. Theoretical framework

Using straightforward symmetry considerations it can be shown that all MO phenomena are caused by the symmetry reduction — compared to the paramagnetic state — caused by magnetic ordering [41]. Concerning optical properties this symmetry reduction only has consequences when SO coupling is considered in addition. To calculate MO properties one therefore has to account for magnetism and SO coupling at the same time when dealing with the electronic structure of the material considered. Performing corresponding band structure calculations it is normally sufficient to treat SO coupling in a perturbative way. A more rigorous scheme, however, is obtained by starting from the Dirac equation set up in the framework of relativistic spin density functional theory [42]:

$$[c\alpha\cdot p + \beta mc^2 + IV + V_{sp}\beta\sigma_z]\,\psi_{n\mathbf{k}} = \varepsilon_{n\mathbf{k}}\psi_{n\mathbf{k}} \quad (1)$$

with $V_{sp}(\mathbf{r})$ the spin-polarized part of the exchange-correlation potential corresponding to the z quantization axis. All other parts of the potential are contained in $V(\mathbf{r})$. The 4×4 matrices α, β and I are defined by

$$\alpha = \begin{pmatrix} 0 & \sigma \\ \sigma & 0 \end{pmatrix}, \quad \beta = \begin{pmatrix} 1 & 0 \\ 0 & -1 \end{pmatrix}, \quad I = \begin{pmatrix} 1 & 0 \\ 0 & 1 \end{pmatrix}, \quad (2)$$

with σ the standard Pauli matrices, and 1 the 2×2 unit matrix.

There are quite a few band structure methods available now that are based on the above Dirac equation [43]. In the first scheme the basis functions are derived from the proper solution to the Dirac equation for the various single-site potentials [44,45]. In the second one, the basis functions are obtained initially by solving the Dirac equation without the spin-dependent term [46,47] and then this term is accounted for only in the variational step [17,44]. In spite of this approximation used, the second scheme nevertheless gives results in very good agreement with the first one [43], while being very simple implemented. We also mention the quite popular technique when SO coupling is added variationally [46] after the scalar relativistic magnetic Hamiltonian has been constructed. In this case only the Pauli equation with SO coupling is being solved. All three techniques yield similar results.

In the polar geometry, where the z-axis is chosen to be perpendicular to the solid surface, and parallel to the magnetization direction, the expression for the Kerr angle can be obtained easily for small angles and is given by [4]

$$\theta_K(\omega) + i\varepsilon_K(\omega) = \frac{-\sigma_{xy}(\omega)}{\sigma_{xx}(\omega)\,[1 + (4\pi i/\omega)\sigma_{xx}(\omega)]^{1/2}}, \quad (3)$$

with θ_K the Kerr rotation and ε_K the so-called Kerr ellipticity. $\sigma_{\alpha\beta}$ ($\alpha, \beta \equiv x, y, z$) is the optical conductivity tensor, which is related to the dielectric tensor $\varepsilon_{\alpha\beta}$ through

$$\varepsilon_{\alpha\beta}(\omega) = \delta_{\alpha\beta} + \frac{4\pi i}{\omega}\sigma_{\alpha\beta}(\omega). \quad (4)$$

The optical conductivity tensor, or equivalently, the dielectric tensor is the important spectral quantity needed for the evaluation of the Kerr effect [5]. The optical conductivity can be computed from the energy band-structure by means of the Kubo-Greenwood [11] linear-response expression [13]:

$$\sigma_{\alpha\beta}(\omega) = \frac{-ie^2}{m^2\hbar V_{uc}} \times$$

$$\times \sum_{\mathbf{k}} \sum_{nn'} \frac{f(\varepsilon_{n\mathbf{k}}) - f(\varepsilon_{n'\mathbf{k}})}{\omega_{nn'}(\mathbf{k})} \frac{\Pi^{\alpha}_{n'n}(\mathbf{k})\,\Pi^{\beta}_{nn'}(\mathbf{k})}{\omega - \omega_{nn'}(\mathbf{k}) + i\gamma} \quad (5)$$

with $f(\varepsilon_{n\mathbf{k}})$ the Fermi function, $\hbar\omega_{nn'}(\mathbf{k}) \equiv \varepsilon_{n\mathbf{k}} - \varepsilon_{n'\mathbf{k}}$, the energy difference of the Kohn-Sham energies $\varepsilon_{n\mathbf{k}}$, and γ is the lifetime parameter, which is included to describe the finite lifetime of excited Bloch electron states. The $\Pi^{\alpha}_{nn'}$ are the dipole optical transition matrix elements, which in a fully relativistic description are given by [49]

$$\Pi_{nn'}(\mathbf{k}) = m\langle\psi_{n\mathbf{k}}|c\alpha|\psi_{n'\mathbf{k}}\rangle \quad (6)$$

with $\psi_{n\mathbf{k}}$ the four-component Bloch electron wavefunction.

Equation 5 for the conductivity contains a double sum over all energy bands, which naturally

separates in the so called interband contribution, i.e., $n \neq n'$, and the intraband contribution, $n = n'$. The intraband contribution to the diagonal components of σ may be rewritten for zero temperature as

$$\sigma_{\alpha\alpha}(\omega) \equiv \frac{(\omega_{p,\alpha})^2}{4\pi} \frac{i}{\omega + i\gamma_D} , \qquad (7)$$

with $\omega_{p,\alpha}$ the components of the plasma frequency, which are given by

$$(\omega_{p,\alpha})^2 \equiv \frac{4\pi e^2}{m^2 V_{uc}} \sum_{n\mathbf{k}} \delta(\varepsilon_{n\mathbf{k}} - E_F) \, |\Pi^{\alpha}_{nn}|^2 , \qquad (8)$$

and E_F is the Fermi energy. For cubic symmetry, we furthermore have $\omega_p^2 \equiv \omega_{p,x}^2 = \omega_{p,y}^2 = \omega_{p,z}^2$. Equation (7) is identical to the classical Drude result for the ac conductivity, with $\gamma_D = 1/\tau_D$, and τ_D the phenomenological Drude electron relaxation time. The intraband relaxation time parameter γ_D may be different from the interband relaxation time parameter γ. The latter can be frequency dependent [48], and, because excited states always have a finite lifetime, will be non-zero, whereas γ_D will approach zero for very pure materials. Here we adopt the perfect crystal approximation, i.e., $\gamma_D \to 0$. For the interband relaxation parameter, on the other hand, we shall use, unless stated otherwise, $\gamma = 0.2$ eV. This value has been found to be on average a good estimate of this phenomenological parameter. The contribution of interband transitions to the off-diagonal conductivity usually is not considered. Also we did not study the influence of local field effects on the MO properties.

We mention, lastly, that the Kramers-Kronig transformation has been used to calculate the dispersive parts of the optical conductivity from the absorptive parts.

The application of standard LDA methods to f-shell systems meets with problems in most cases, because of the correlated nature of the f electrons. To account better for the on-site f-electron correlations, we have adopted as a suitable model Hamiltonian that of the LDA+U approach [50]. The main idea is the same as in the Anderson impurity model [51]: the separate treatment of localized f-electrons for which the Coulomb f-f interaction is taken into account by a Hubbard-type term in the Hamiltonian $\frac{1}{2} U \sum_{i \neq j} n_i n_j$ (n_i are f-orbital occupancies), and delocalized s, p, d electrons for which the local density approximation for the Coulomb interaction is regarded as sufficient.

Let us consider the f ion as an open system with a fluctuating number of f electrons. The formula for the Coulomb energy of f-f interactions as a function of the number of f electrons N given by the LDA is $E = UN(N-1)/2$. If we subtract this expression from the LDA total energy functional, add a Hubbard-like term and take into account the exchange interaction we obtain the following functional [50]:

$$E = E_{LDA} + \frac{1}{2} U \sum_{m,m',\sigma} n_{m\sigma} n_{m'-\sigma} +$$

$$+ \frac{1}{2} (U - J) \sum_{m \neq m',m',\sigma} n_{m\sigma} n_{m'\sigma} - \text{d.c.} , \qquad (9)$$

where

$$\text{d.c.} = U \frac{N(N-1)}{2} - \frac{JN^{\uparrow}(N^{\uparrow} - 1)}{2} - \frac{JN^{\downarrow}(N^{\downarrow} - 1)}{2} ,$$

N is the total number of localized f electrons; $N^{\uparrow}$ and $N^{\downarrow}$ are the number of f electrons with spin-up and spin-down, respectively; U is the screened Coulomb parameter; J is the exchange parameter.

The orbital energies ε_i are derivatives of (9) with respect to orbital occupations n_i :

$$\varepsilon_i = \frac{\partial E}{\partial n_i} = E_{LDA} + (U - J)\left(\frac{1}{2} - n_i\right) =$$

$$= E_{LDA} + U_{\text{eff}}\left(\frac{1}{2} - n_i\right). \qquad (10)$$

This simple formula gives the shift of the LDA orbital energy $-U_{\text{eff}}/2$ for occupied f orbitals ($n_i = 1$) and $+U_{\text{eff}}/2$ for unoccupied f orbitals ($n_i = 0$). A similar formula is found for the orbital dependent potential $V_i(\mathbf{r}) = \delta E/\delta n_i(\mathbf{r})$, where variation is taken not on the total charge density $\rho(\mathbf{r})$ but on the charge density of a particular ith orbital $n_i(\mathbf{r})$:

$$V_i(\mathbf{r}) = V_{LDA}(\mathbf{r}) + U_{\text{eff}}\left(\frac{1}{2} - n_i\right). \qquad (11)$$

The advantage of the LDA+U method is the ability to treat *simultaniously* delocalized conduction band electrons and localized 4f- electrons in the same computational scheme. With regard to these electronic structure calculations, we mention that the present approach is still essentially a single particle description, even though intraatomic 4f-Coulomb correlations are explicitly taken into account.

The LDA+U method has proven to be a very efficient and reliable tool in calculating the electronic structure of systems containing localized orbitals where the Coulomb interaction is much larger than the band width. It works not only for 4f

orbitals of rare-earth ions, but also for such systems as transition metal oxides, where localized 3*d* orbitals hybridize quite strongly with oxygen 2*p* orbitals (see review article Ref. 52). The LDA+U method was recently applied to heavy-fermion compounds YbPtBi [53] and Yb_4As_3 [54] and it has also to explain the nature of colossal polar Kerr rotation of the maximal possible rotation of 90° in CeSb (Ref. 33).

We should also note that for large Kerr rotation, it is not possible to use the approximate expression (3) for the polar Kerr rotation. This equation is valid only for small θ_K , ε_K , and $|\varepsilon_{xy}| << |\varepsilon_{xx}|$. Instead one must use the *exact* expression

$$\frac{1+\tan\varepsilon_k}{1-\tan\varepsilon_K}\, e^{2i\theta_K} = \frac{1+n_+}{1-n_+}\,\frac{1-n_-}{1+n_-} \qquad (12)$$

with $n_\pm = (\varepsilon_{xx} \pm i\varepsilon_{xy})^{1/2}$, the complex indices of refraction. From Eq. 12 it can be seen that the maximal observable θ_K is ± 90°.

2. 3*d*- transition-metal compounds

Transition-metal alloys consisting of a ferromagnetic 3*d* elements have drawn attention over the last years because of their good magneto-optical (MO) properties (see, e.g., Refs. 55–57). Especially multilayers of Co and Pt or Pd are at present intensively studied because of their potential application as optical storage material in MO storage devices [58–60]. In addition to this, it has recently been discovered that the compound $MnPt_3$ exhibited a very large MO Kerr rotation, of about −1.2° at 1 eV photon energy [61,62]. This discovery indicates that the whole group of transition-metal-platinum alloys is exceptionally interesting within MO research, and also that large Kerr effects might still be found in materials which were previously not considered for their MO properties.

With the aim of undertaking a systematic investigation of the trends in transition-metal alloys, we study (in the present work) theoretically the MO Kerr spectra of the series XPt_3 compounds (with *X* = V, Cr, Mn, Fe, and Co), Heusler alloys (PtMnSb, PdMnSb and NiMnSb) and MnBi.

2.1. XPt_3 *compounds* (*X* = V, Cr, Mn, Fe, *and* Co)

The calculated polar Kerr spectra of VPt_3 , $CrPt_3$, and $MnPt_3$ are shown in Fig. 1, and those of $FePt_3$ and $CoPt_3$ in Fig. 2. All Kerr spectra given in Figs. 1 and 2 pertain to the (001) magnetization direction, and are due to the interband optical conductivity tensor only, i.e., no free-electron contributions to the conductivity are considered. A Lorentzian broadening with a half width at a half maximum of 0.4 eV, taking account of the effects of finite lifetimes and of the experimental resolution, has been applied to all optical conductivity spectra. In Fig. 1, the recently measured Kerr spectra of $MnPt_3$ are also shown [61]. As one can see from Figs. 1 and 2, the Kerr spectra of VPt_3 , $CrPt_3$, and $MnPt_3$ are very similar, as are those of $FePt_3$ and $CoPt_3$. This is the reason why we show the spectra in this combination together. The theoretical Kerr rotations of VPt_3 , $CoPt_3$, and $MnPt_3$ have their minimum at the same photon energy of 0.8 eV, followed by a zero crossing at 2 eV. This similarity is partially observed in the Kerr ellipticity too. The Kerr rotations of $FePt_3$ and $CoPt_3$,

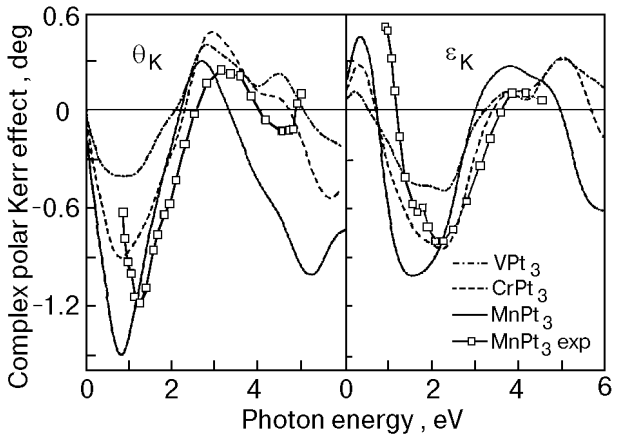

Fig. 1. Calculated polar Kerr rotation (θ_K) and Kerr ellipticity (ε_K) spectra of VPt_3 , $CrPt_3$, and $MnPt_3$ in the $AuCu_3$ crystal phase with (001) magnetization orientation. The theoretical spectra are all calculated with a relaxation-time broadening of 0.4 eV and result from the interband optical conductivity only. The experimental data shown are those of $MnPt_3$ (Ref. 61).

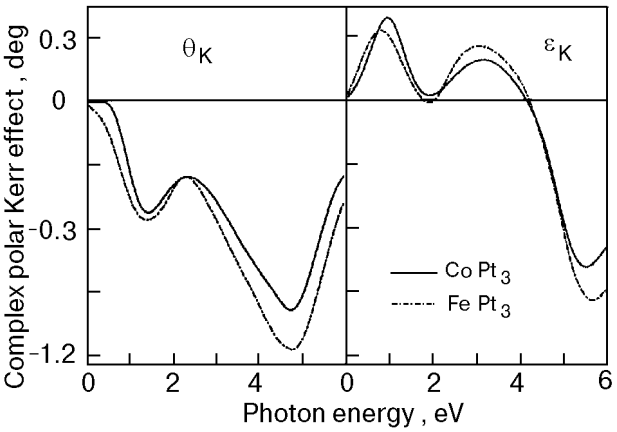

Fig. 2. As Fig. 1, but for the theoretical polar Kerr spectra of $FePt_3$ and $CoPt_3$.

however, are distinctly different, as they have no zero crossing, and exhibit two minima, one smaller minimum at 1.3 eV, and a larger one at 4.7 eV. Noticeable further are the large Kerr rotations that are predicted by density-functional theory for these compounds. The largest Kerr rotation is found for $MnPt_3$ which reaches a value of $-1.5°$ at 0.8 eV. But also the Kerr rotation of the $CrPt_3$ alloy as yet not investigated is surprisingly large, being with a peak value of $-0.9°$ at 0.8 eV larger than that of the transition metals Fe and Co. Further the Kerr rotations predicted for $FePt_3$ and $CoPt_3$ are with peak values of $-1.0°$ to $-1.1°$ at 4.7 eV also substantial. (The term «peak» is used for a maximal Kerr rotation, irrespective of whether it is of positive or negative sign.) With respect to the magnitudes of the Kerr rotations displayed in Figs. 1 and 2, there are three points to be mentioned. First, the precise peak magnitude depends on the applied broadening parameter. A larger broadening than 0.4 eV would generally lead to slightly smaller, but broader spectral peaks. However, so far it is our experience that the broadening parameter of 0.4 eV gives a physically adequate description [21]. Second, the neglect of an intraband contribution to the optical conductivity can play a role for VPt_3 , $CrPt_3$, and $MnPt_3$. An intraband or free-electron contribution to the optical conductivity can be of importance for the Kerr rotation spectrum at small photon energies. As the main Kerr rotation peak of the compounds in Fig. 1 occurs at a small energy, the size of this peak will become reduced when a large intraband contribution is present. For $CoPt_3$ and $FePt_3$, the intraband contribution is less important, because these compounds already have a relatively small Kerr rotation at low energies (see Fig. 2). Third, it should be noted that the *ab initio* Kerr spectra are essentially calculated for zero temperature. If the Kerr spectra are measured at room temperature, where the magnetization is smaller, then the over-all size of the thus measured Kerr rotation will be smaller too. In Fig. 1 also the recently measured Kerr spectra of ordered $MnPt_3$ are shown [61,62]. These spectra were measured from an annealed thin film of $MnPt_3$ on a quartz substrate, but from the substrate side, i.e., through quartz [61]. This implies that these can be enhanced over the Kerr spectra measured in air by a factor of about one and a half. Within the limitations concerning the size of the Kerr rotation mentioned above, and the possible influence of the quartz substrate on the Kerr spectra, it can only be concluded that the shape of the theoretical and experimental Kerr rotation and ellipticity spectra are in good agreement as yet.

Density-functional theory predicts a large Kerr effect in the XPt_3 alloys. Noticeably, the Kerr rotations predicted are much larger than those calculated for, e.g., Fe, Co, or Ni, where the same broadening parameter of 0.4 eV was used. An important issue is therefore to identify the origin of the large Kerr effect in these compounds. To this end, we examine the dependence of the MO spectra on the exchange splitting, the SO interaction, and the optical transition matrix elements. As it can be expected that the Kerr effect in each of these compounds is of the same origin, we do this only for one compound, $CrPt_3$. The exchange splitting and the SO coupling are studied by scaling the corresponding terms in the Hamiltonian artificially with a constant prefactor. This is done in a non-self-consistent way, i.e., after self-consistency has been achieved, only one iteration is performed with the modified Hamiltonian (a self-consistent calculation would lead to a different band structure). From the resulting band structure the optical spectra are then computed. These modifications can in addition be done atom dependent, i.e., within each atomic sphere, so that we can investigate the separate effects of these quantities on Cr and on Pt. The outcomes of these model calculations for the Kerr rotation of $CrPt_3$ are shown in Fig. 3. In the upper panel, the importance of the exchange splitting is illustrated. When the exchange splitting on Pt is set to zero, the Kerr rotation remains as it is But when we do the same for the exchange splitting on Cr, the Kerr rotation totally vanishes. This implies that the exchange splitting due to Cr is crucial for the sizeable Kerr rotation, but that of Pt is unimportant. Furthermore, an enhancement of the exchange splitting on Cr by a factor of two (dashed line) leads to a much larger peak in the Kerr rotation. The middle panel in Fig. 3 shows the dependence on the SO coupling. If we set the SO coupling on Cr to zero, the Kerr rotation practically doesn't change (dotted line). On the other hand, when the SO coupling on Pt is zero, the Kerr rotation almost disappears (dashed line). Thus, the SO coupling of Pt is equally responsible for the large Kerr rotation as is the exchange splitting of Cr. An intermediate scaling of the SO coupling of Pt by a factor of 0.5 leads to an approximately half as large Kerr angle, thereby illustrating the almost linear dependence of the Kerr effect on the SO interaction of Pt in these compounds. The lower panel in Fig. 3, finally, displays the importance of the site-dependent matrix elements. Within an

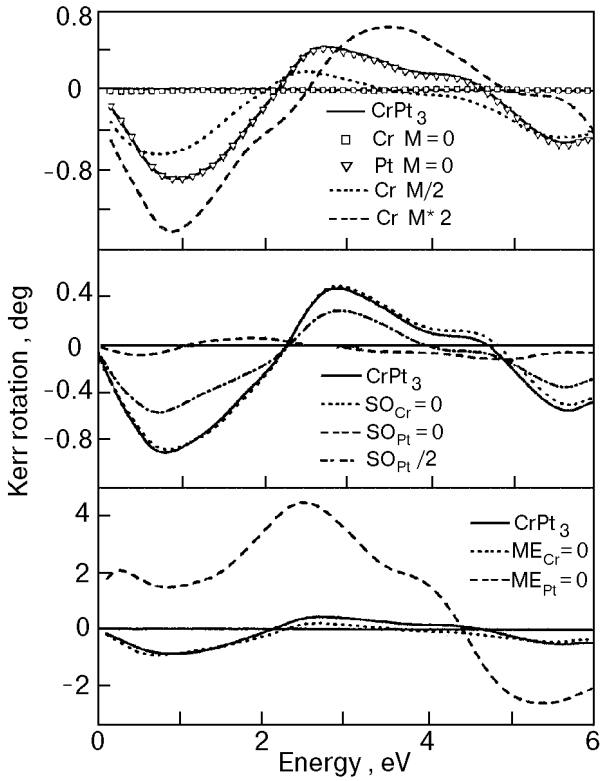

Fig. 3. Study of the influence of the exchange splitting (M), spin-orbit (SO) coupling, and optical transition matrix elements (ME) on the Kerr rotation of $CrPt_3$. The upper panel shows the effect of multiplying the spin-polarized part of the Dirac Hamiltonian with a constant factor, on the Cr site or on the Pt site. The middle panel shows the effect of multiplying the SO-coupling part of the Hamiltonian on Cr or on Pt with a constant prefactor (see text). The lower panel depicts the effect of setting the matrix elements on Cr or on Pt to zero.

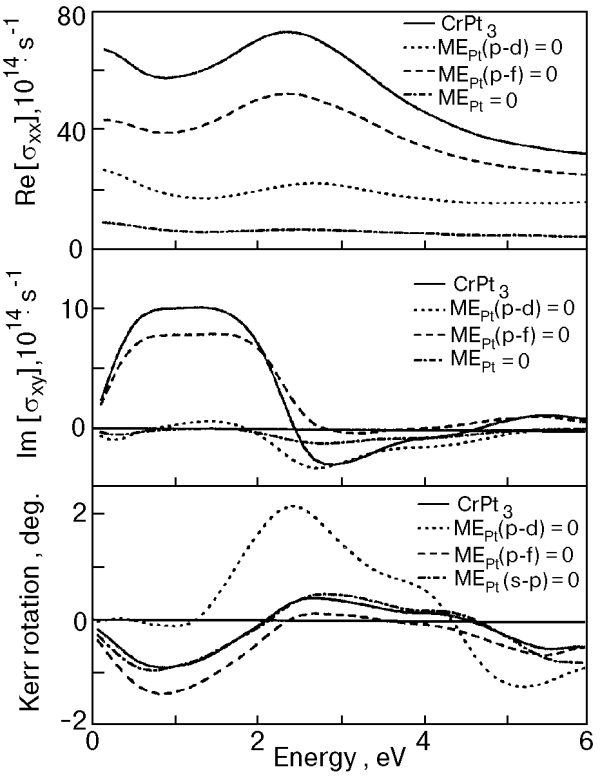

Fig. 4. Influence of the exclusion of various optical matrix elements on the Pt site on the real part of the diagonal optical conductivity ([Re [σ_{xx}]), the imaginary part of the off-diagonal optical conductivity (Im [σ_{xy}]) and Kerr rotation. The notation $ME_{\mathrm{Pt}}\,(p\text{–}d) = 0$ means that on the Pt site the *p-d* interband transitions and the *d-p* interband transitions are excluded from the optical matrix element.

atomic sphere about one of the atomic positions, the optical transition matrix elements are set to zero. If this is done for the matrix elements on Cr, the Kerr rotation doesn't change much. But if the matrix elements on Pt vanish, a large impact on the Kerr rotation is found (dashed curve). This indicates that the matrix elements on the Pt site are more important for bringing about the large Kerr peak at 1 eV, than are those of Cr. Making the matrix elements zero gives only an impression of which site the main contribution comes from. To obtain information about the bands that are responsible for the Kerr peak, it is instructive to exclude a particular transition matrix element. Due to the selection rules for optical transitions, these transitions can only take place between band states with an angular momentum difference of ± 1. By excluding for instance the *p-d* transition matrix element we can investigate the contribution of this type of transitions. However, as the transition matrix must be Hermitian, we have to exclude also the conjugated transition, i.e., both *p-d* and *d-p* transitions. The results of an investigation of the importance of the various transitions on Pt are shown in Fig. 4, for the real part of the diagonal optical conductivity, Re [σ_{xx}], the imaginary part of the off-diagonal conductivity, Im [σ_{xy}], and the Kerr rotation. The upper and middle panel in Fig. 4 show that both Re [σ_{xx}] and Im [σ_{xy}] are strongly reduced when the *p-d* and *d-p* interband transitions are excluded, more than when the *d-f* and *f-d* transitions are excluded. Especially the off-diagonal conductivity almost disappears in the energy region around 1 eV if the *p-d* and *d-p* transitions on the Pt sites are excluded. Because this peak in the off-diagonal conductivity at 1 eV is responsible for the peak in the Kerr rotation spectrum, this shows that the *d-p* and *p-d* transition matrix elements on Pt account for most of the Kerr effect in this frequency region. The other transitions, *s-p* and *d-f*, also have a minor influence, but excluding these still gives approximately the same Kerr rotation (see Fig. 4, lower panel). Thus, the *d* states of Pt, being subject to the strong SO interaction on the Pt site, contribute

most to the optical transitions that lead to a large Kerr angle.

From these investigations the following picture of the Kerr effect in these compounds emerges: Pt is the magneto-optically active element, and creates the large Kerr rotation through its large SO interaction. The important magneto-optical transitions are the p-d and d-p transitions on Pt. The $3d$ elements are magneto-optically not very active. Their role is to supply through their exchange splitting enough hybridized spin-split energy bands. This understanding suggests the following recipe for finding a material having a sizeable Kerr rotation: such material should contain elements with a large SO coupling, for instance Pt, Bi, or an actinide. Also should it contain an element having a sufficiently large magnetic moment, but this element needn't have a strong SO interaction, like for instance Mn. Also should there be a substantial hybridization between states of these two kinds of constituents. Elements having a large, but local atomic moment, like some of the $4f$-elements, are in the latter respect not suited, if the moment is due to unhybridized, localized $4f$-states.

The behavior of the peak magnitude in the Kerr rotation spectra with respect to th $3d$ element, as shown in Figs. 1 and 2, and also the dependence of the Kerr effect magnitude on the magnetization, can furthermore be understood on the basis of the model calculations. The increase of the peak in the Kerr angle at about 1 eV when going from VPt_3 to $MnPt_3$ (see Fig. 1) is caused by the corresponding increase in the exchange splitting. This is most clearly demonstrated by the scaling of the peak in the Kerr rotation of $CrPt_3$ with respect to the scaling of the exchange splitting (Fig. 3, upper panel). Also it can be understood from this behavior that a reduction of the magnetization at room temperature leads to a reduction of the Kerr rotation. This dependence on the magnetization also explains why the Kerr rotation of $FePt_3$ is larger than that of $CoPt_3$.

In concluding, we have further proven the important result that the total density of states cannot be used to derive information about the shape or magnitude of the Kerr spectra thereof. The dependence of the Kerr spectra in the XPt_3 compounds on the crystallographic direction of the magnetization is found to be very small. This finding corroborates with the high degree of isotropy of the $AuCu_3$ crystal structure. The agreement between the *ab initio* calculated Kerr spectra and the experimental result for $MnPt_3$ (Ref. 61, 62) finally looks very promising. Further measurements on these compounds are desirable and needed, in order to obtain a complete picture of the correspondence between experimental and first-principles Kerr spectra.

2.2. Heusler alloys

The Heusler alloys NiMnSb, PdMnSb, and PtMnSb have been the subject of intensive experimental and theoretical investigations since the early 1980's [55,63–65]. The interest in these compounds arose first from the experimental discovery of an extremely large magneto-optical Kerr rotation of $-1.27°$ in PtMnSb at room temperature [55]. This value was for many years the record Kerr rotation observed in a transition metal compound at room temperature and therefore called «giant» Kerr effect (see, e.g., the recent surveys Refs. 3, 5). Almost simultaneously with the experimental discovery, the theoretical finding of the so-called «half-metallic» nature of PtMnSb was reported [65]. Half-metallicity means that according to (semirelativistic) bandstructure theory the material is metallic for majority, but insulating for minority spin electrons [65]. Such a gap for one spin type naturally may give rise to unusual magnetotransport and optical properties. Also the isoelectronic Heusler alloy NiMnSb was predicted to be half-metallic, whereas the isoelectronic compound PdMnSb was predicted not to be half-metallic [65]. The MO Kerr rotations in both NiMnSb and PdMnSb on the other hand, were experimentally found to be much smaller than that of PtMnSb, which resulted in a puzzling combination of features. Experimental efforts were undertaken to verify the proposed half-metallic character of NiMnSb and PtMnSb [66–69], which was subsequently established in the case of NiMnSb [66,69]. Very recently, also experimental evidence in favor of half-metallicity in PtMnSb was reported [70].

On the theoretical side, several model explanations of the MO spectra of the compounds were proposed [71–73]. One of those was based on a possible loss of the half-metallic character due to spin-orbit (SO) coupling which was suggested to lead to a symmetry breaking between the different m states of the Sb p bands in the vicinity of the Fermi energy E_F [71]. Another explanation was based on differences of the semirelativistic effects in NiMnSb and PtMnSb [73], and another one on enhancement of the MO Kerr spectra near the plasma resonance [72]. While the proposed models contain interesting physical mechanisms themselves, one of the remaining major stumbling blocks was to explain the measured differences in the MO

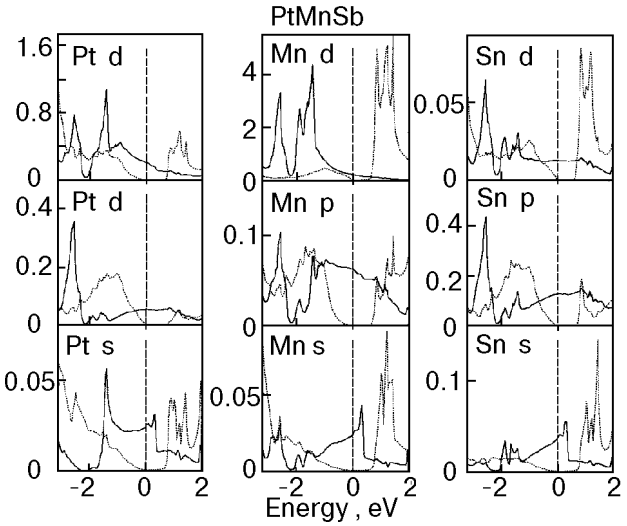

Fig. 5. Spin-projected, partial densities of state calculated for PtMnSb. Majority spin densities are given by the full curves, minority spin densities by the dotted curves. The half-metallic behavior can be seen from the band gap at the Fermi level, which is present for minority spin, but not for majority spin.

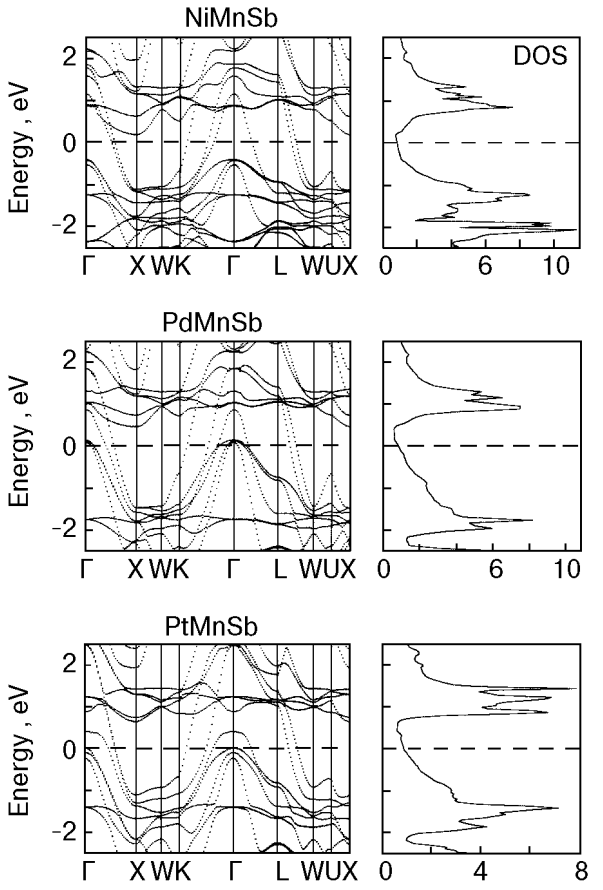

Fig. 6. Relativistic, spin polarized energy bandstructures and total densities of state (DOS) of NiMnSb, PdMnSb, and PtMnSb.

spectra of the isoelectronic NiMnSb, PdMnSb, and PtMnSb.

Only owing to the development of *ab initio* calculations of the MO spectra the detailed quantitative comparison between experiment and first-principles spectra became feasible [15–17,74, 75]. The Heusler compounds are, of course, most attractive materials for *ab initio* calculations of their MO spectra on account of the mentioned unusual features. Several first-principles calculations for these compounds were reported very recently [15,18,21, 26,31]. The various calculated MO Kerr spectra, however, spread rather widely. The origin of the differences in the spectra obtained in the various calculations traces back, first, to the fact that the MO Kerr effect is in calculations a tiny quantity, related to the difference of reflection of left- and right-hand circularly polarized light [5]. SO coupling in the presence of spontaneous magnetization is responsible for the symmetry breaking in the reflection of left- and right-hand circularly polarized light. Second, since the MO Kerr effect is only a tiny quantity in the first-principles calculations, numerical accuracy and the influence of approximations made in the evaluation gain an appreciable importance. For this reason, the evaluation of the MO Kerr spectra of the ferromagnetic 3*d* transition metals Fe, Co, and Ni have become bench mark test cases for MO calculation schemes [16,17, 75–79]. Numerical accuracy plays normally not a decisive role if the physical mechanism is to be sought. However, it has been shown by several groups [16,75] that for the *ab initio* calculation of MO spectra an accurate evaluation of the dipole matrix elements is essential for obtaining numerically reliable MO Kerr spectra. Moreover, in the particular case of the Heusler alloys, the half-metallic band gap depends sensitively on technicalities of the band structure calculation, as, e.g., atomic sphere radii [21].

In the present work we report a detailed investigation of the MO Kerr spectra of NiMnSb, PdMnSb, and PtMnSp [26].

Figure 5 shows the spin projected, fully relativistic partial densities of states of PtMnSb. As can be recognized from Fig. 5, the partial densities of states for minority spin have evidently a gap at the Fermi level. A similar behavior we have found for NiMnSb, but, of course, not for PdMnSb. For all three Heusler compounds we show the calculated relativistic energy bands and total densities of state (DOS) in Fig. 6. In the case of PdMnSb, three spin-orbit split energy bands are just above the Fermi level at the Γ-point, therefore half-metallic behavior is not supported for PdMnSb by band-

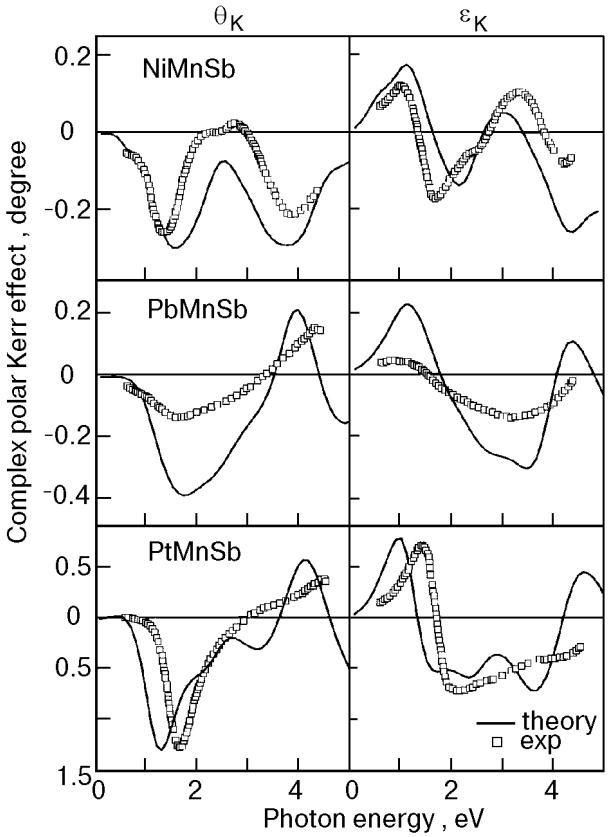

Fig. 7. Calculated and experimental Kerr rotation (θ_K) and Kerr ellipticity (ε_K) spectra of the Heusler compounds NiMnSb, PdMnSb, and PtMnSb. The experimental data are those of Refs. 55,64.

structure theory. In the case of NiMnSb and PtMnSb, these important bands are just below E_F, rendering the half-metallicity in these compounds. Our bandstructure results are in agreement with recent experiments on NiMnSb and PtMnSb, in which half-metallic behavior to a degree of nearly 100% was observed [66,69,70].

After having verified the half-metallic bandstructure property we turn to the magneto-optical spectra. In Fig. 7 we show the calculated and experimental [55,64] MO Kerr spectra of the three isoelectronic Heusler compounds. There exists apparently a rather good agreement between the experimental Kerr spectra and the *ab initio* calculated ones. Overall, the experimental features are reasonably well reproduced, except for the magnitude of the Kerr rotation of PdMnSb, for which theory predicts larger values than are experimentally observed. The first and important conclusion which we draw from the correspondence between experimental and calculated Kerr spectra is: *the anomalous behavior of the MO Kerr spectra in these compounds is well described by normal bandstructure theory*. While the calculated MO Kerr spectra of these three Heusler compounds were recently shown in a review paper [18], an explanation in detail of the origin of the depicted spectra has not yet been given we shall give it in the following.

To investigate the origin of the Kerr spectra, we consider the separate contributions of both the numerator of Eq. (3), i.e., $\sigma_{xy}(\omega)$ and the denominator, $D(\omega) \equiv \sigma_{xx}(1 + \sigma_{xx} 4\pi i/\omega)^{1/2}$. In Fig. 8 we show how the separate contributions of numerator and denominator bring about the Kerr angle of NiMnSb. The imaginary part of the inverse denomi-

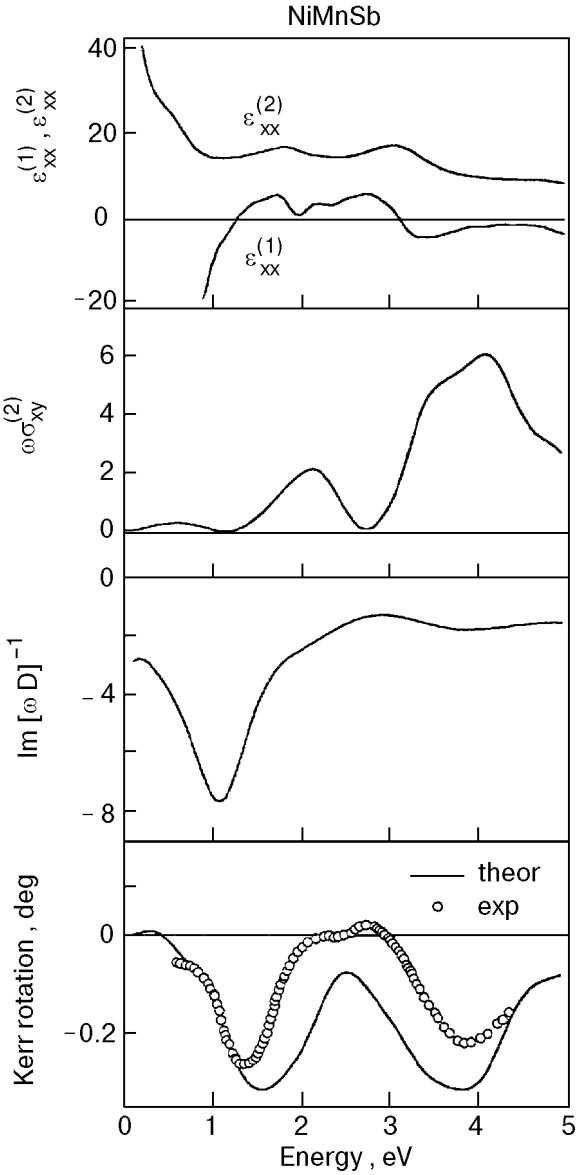

Fig. 8. Decomposition of the Kerr rotation spectrum of NiMnSb in separate contributions. Top panel: calculated real and imaginary part of the diagonal dielectric function, $\varepsilon_{xx}^{(1)}$ and $\varepsilon_{xx}^{(2)}$, respectively. Third panel from the top: the imaginary part of $[\omega D]^{-1}$ which results from $\varepsilon_{xx}^{(1)}$ and $\varepsilon_{xx}^{(2)}$. Bottom panel: the Kerr rotation which results as a combination of Im $[\omega D]^{-1}$ and $\omega\sigma_{xy}^{(2)}$ (second panel from the top). The experimental Kerr angle spectrum is after van Engen et al. [55].

nator (times the photon frequency), $\mathrm{Im}\,[\omega D]^{-1}$, displays a typical resonance structure at about 1 eV. The imaginary part of $\omega\sigma_{xy}$, i.e., $\omega\sigma^{(2)}_{xy}$ displays a double peak structure. The double peak structure of the Kerr rotation results roughly as the product of $\mathrm{Im}\,[\omega D]^{-1}$ and $\omega\sigma^{(2)}_{xy}$. The first peak in the Kerr rotation at 1.5 eV is predominantly caused by a minimum of the denominator, whereas the second peak in the Kerr rotation at 4 eV is due to a maximum in the off-diagonal conductivity, $\omega\sigma^{(2)}_{xy}$. The nature of the peak in $\mathrm{Im}\,[\omega D]^{-1}$ can be understand from the top panel in Fig. 8, where the complex diagonal dielectric function is shown: its real part, $\varepsilon^{(1)}_{xx}$, becomes small at about 1 eV, and its imaginary part, $\varepsilon^{(2)}_{xx}$, has a shallow minimum at 1 eV. The second peak in the Kerr rotation, stems from the maximum in $\omega\sigma^{(2)}_{xy}$, which in turn is known to be due to the interplay of SO coupling and spin polarization [8,18]. Thus, the two similar looking peaks in the Kerr rotation arise in fact from quite a different origin.

Next, we consider the spectra for the compound PdMnSb in more detail, which are shown in Fig.9. In this compound $\omega\sigma^{(2)}_{xy}$ is larger than that of NiMnSb in the energy range 1–4 eV. This is simply due to the larger SO interaction on Pd as compared to that on Ni. The inverse denominator $\mathrm{Im}\,[\omega D]^{-1}$, however, does not exhibit such a strong resonance as it does for NiMnSb. The latter is related to the particular shape of the $\varepsilon^{(1)}_{xx}$ and $\varepsilon^{(2)}_{xx}$ spectra. The Kerr rotation in effect displays the same shape as

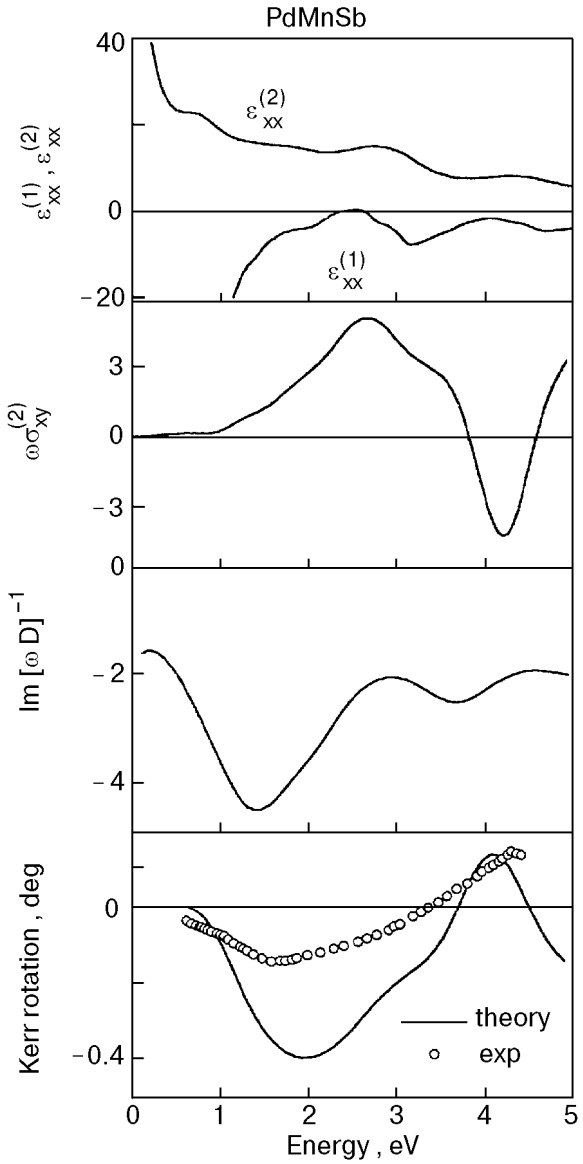

Fig. 9. As Fig. 8, but for PdMnSb.

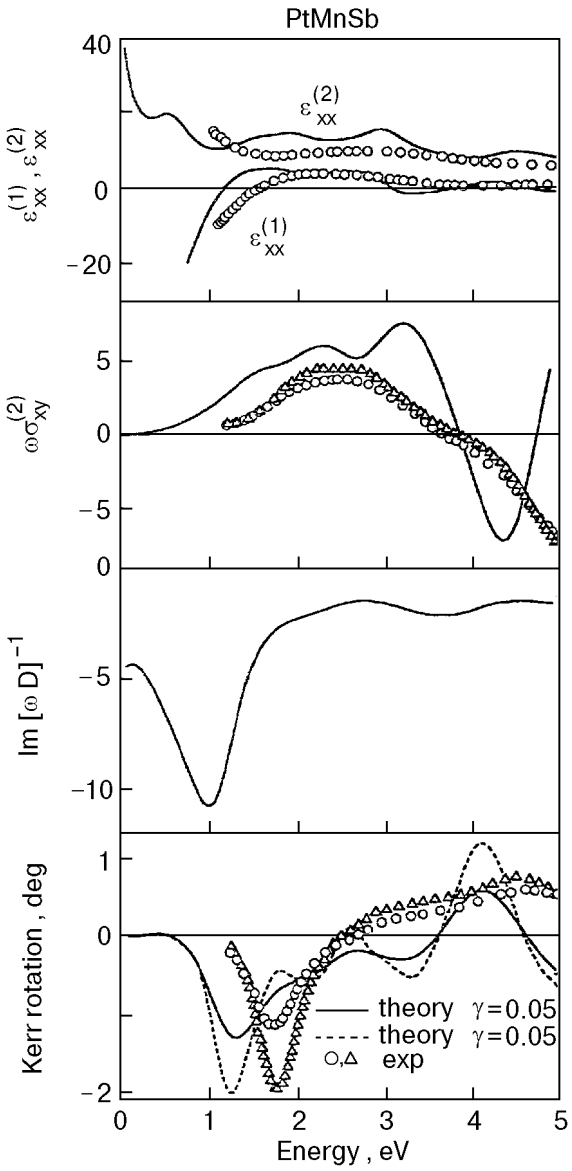

Fig. 10. As Fig. 8, but for PtMnSb. The experimental data are after Ikekame et al. [88]. The data for annealed PtMnSb are denoted by Δ, and those for non-annealed, polished PtMnSb by ❍. The calculated Kerr rotation spectrum is shown for two interband lifetime parameters, $\gamma = 0.05$ Ry and $\gamma = 0.02$ Ry.

$\omega\sigma_{xy}^{(2)}$, being enhanced at 1–2 eV by the contribution from the denominator.

In Fig. 10 we show the spectral quantities for PtMnSb. The inverse denominator Im $[\omega D]^{-1}$ again displays for PtMnSb a strong resonance at 1 eV, which is even larger than that for NiMnSb. In addition, the off-diagonal conductivity $\omega\sigma_{xy}^{(2)}$ is for PtMnSb again larger than that of PdMnSb, in accordance with the larger SO coupling on Pt. The resulting Kerr rotation has a «giant» peak of $-1.2°$ up to $-2.0°$ depending on the applied lifetime parameter (see Fig. 10). These values are in good agreement with the available experimental Kerr peak values for PtMnSb, which range from about $-1°$ to $-2°$ depending on sample preparation and surface quality [55,80–88]. Careful investigations of the consequences of sample preparation have been performed by Takanashi et al. [83] and Sato et al. [87,88]. These investigations showed that annealing of the PtMnSb sample rises the Kerr angle to a maximum value of $-2°$, whereas the non-annealed Kerr angle is only $-1.2°$. The off-diagonal conductivity $\omega\sigma_{xy}^{(2)}$ was found to be rather insensitive to annealing (see. Fig. 10) [87,88]. The main impact of annealing thus evidently occurs in the denominator. The reason for the calculated resonance in the inverse denominator lies again in the frequency dependence of the diagonal dielectric function, which is shown in the top panel of Fig. 10. The calculated ε_{xx} compares reasonably well with the experimental one [88], except for the important first root frequency of $\varepsilon_{xx}^{(1)}$ which is shifted by about 0.5 eV. This difference leads to a shifted position in the resonance peak of Im $[\omega D]^{-1}$, which in turn results in a shifted main Kerr rotation peak of just the same amount. The position of the maximum in Im $[\omega D]^{-1}$ thus predominantly determines the position of the main Kerr rotation peak. We mention in addition that the second maximum in the calculated $\omega\sigma_{xy}^{(2)}$ at 4.4 eV (see Fig. 10) is also present in the experimental spectrum, but at a higher energy of 5.2 eV [88].

The origin of the giant Kerr angle in PtMnSb as compared to the Kerr angles in NiMnSb and PdMnSb can completely be understood from our calculations. First, in these three compounds the off-diagonal conductivities $\sigma_{xy}(\omega)$ are quite different, what is a direct result of the different relativistic electronic structure. Although both NiMnSb and PtMnSb are half-metallic, their $\omega\sigma_{xy}^{(2)}$ spectra are distinctly different, while on the other hand the $\omega\sigma_{xy}^{(2)}$ of PdMnSb and PtMnsb have a similar structure, but not a similar magnitude (see Figs. 8–10). Second, there is the influence of the denominators as exemplified in Im $[\omega D]^{-1}$. These are similar in shape and magnitude for NiMnSb and PtMnSb, but the magnitude of Im $[\omega D]^{-1}$ in PdMnSb is about a factor of two smaller. We find that this difference relates to the half-metallic nature of both NiMnSb and PtMnSb, which is not present for PdMnSb. From Fig.6 it can be seen that for the half-metallic compounds there are three lesser bands at E_F. One consequence is therefore that the intraband contribution to σ_{xx} will be smaller (see Eq. (8)). In Fig. 11 we show the impact of the half-metallic character of the bandstructure on the Kerr rotation of PtMnSb. The calculated plasma frequency in PtMnSb is small, $\hbar\omega_p = 4.45$ eV. Experimentally a

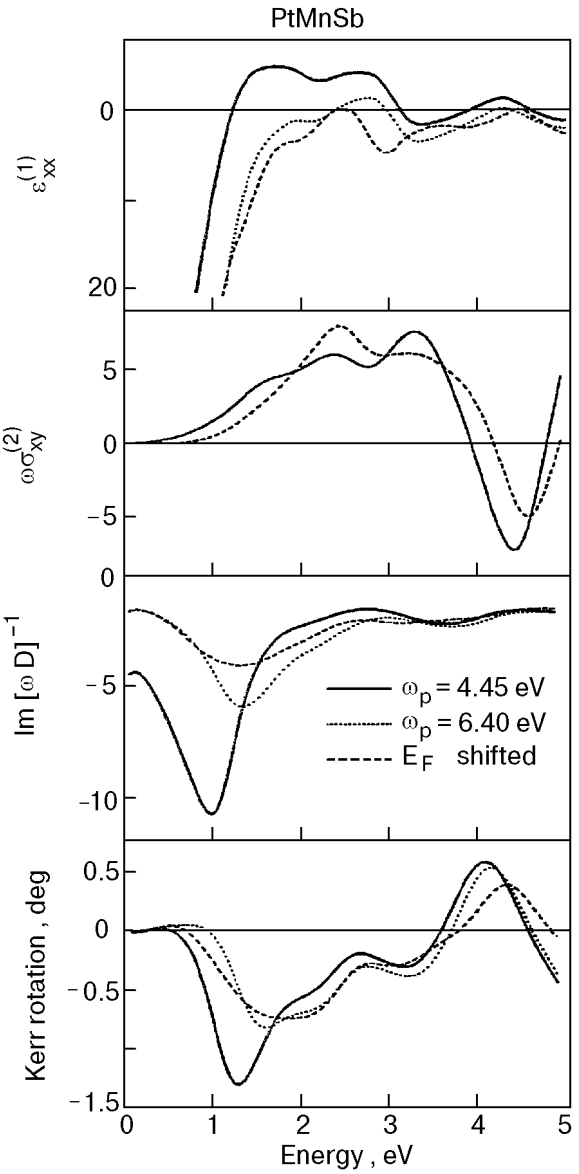

Fig. 11. Model investigation of the influence of the half-metallic character of PtMnSb on the optical and MO spectra. A non-half-metallic bandstructure has been modeled in two ways: by artificially shifting E_F in PtMnSb down, and by increasing the calculated plasma frequency $\omega_p = 4.45$ eV to 6.40 eV.

somewhat bigger plasma frequency of (6.1 ± 0.4) eV was found for PtMnSb, and a smaller $\hbar\omega_p$ = = (4.9 ± 0.2) eV for NiMnSb [89]. One should, however, not forget that the sample purity can affect the plasma frequency through the position of E_F . To investigate the influence of the half-metallicity, we can artificially shift the Fermi energy down, and calculate the spectra for this position of E_F or we can leave E_F as it is and model a non-half-metallic bandstructure by adopting a larger ω_p . Both ways to mimic non-half-metallicity have a drastic impact on the resulting Kerr rotation, which becomes reduced by a factor 2! As can be seen from the top panel in Fig. 11, in the absence of half-metallicity the shape of $\varepsilon_{xx}^{(1)}$ changes and resembles closely that of PdMnSb (see Fig. 9). This is especially so for the model where E_F is shifted, since this leads to the smaller Im $[\omega D]^{-1}$ and also to a reduction of $\omega\sigma_{xy}^{(2)}$ at photon energies below 2 eV. The later is due to the exclusion of optical transitions from the SO split bands just below E_F . The consequence of both models for non-half-metallic behavior is that the maximum in Im $[\omega D]^{-1}$ becomes about two times smaller. The Kerr angles derived in these models resemble now that of PdMnSb in shape, but are bigger, because $\omega\sigma_{xy}^{(2)}$ is larger than that of PdMnSb. Previously we have shown that if the SO coupling on Pt in PtMnSb is artificially set to zero, the Kerr rotation peak in PtMnSb becomes reduced by a factor of three [21]. We mention with respect to the influence of the denominator on the Kerr rotation in PtMnSb, that experiments in which the stoichiometry and crystalline sample quality were varied also concluded that the denominator contributed appreciably to the giant Kerr rotation [83,85–88].

In conclusion, we find that the Kerr spectra of NiMnSb, PdMnSb, and PtMnSb can be fully understood from their electronic structure. The puzzling anomalies in the Kerr spectra of these compounds arise from an interplay of compound related differences in the SO interaction, in the half-metallic character, and also in relative positions of energy bands.

2.3. MnBi

Although the MO Kerr effect in MnBi was measured already about twenty years ago, only very recently a thorough investigation of the spectral dependency of the Kerr effect under variation of the Mn-Bi composition [90]. These experimental Kerr spectra obtained at 85 K as well as the calculated ones are shown in Fig. 12. First-principles theory predicts a very large Kerr rotation in MnBi of about −1.75° at 1.8 eV [24], which is even larger than the measured peak value of −1.6° [90]. The lifetime broadening parameter γ used was 0.04 Ry (i.e., γ is the half- width at half maximum of a Lorentzian). However, we wish to point out that a smaller (but still reasonable) relaxation time broadening of 0.02 Ry would already result in a theoretical peak value of −2.22°. Therefore, according to theory, a larger Kerr effect than measured as yet should be possible. Experiment shows a second maximum in the Kerr angle at 3.4 eV, where theory only gives a smaller shoulder. A tentative explanation of this difference might be the sample composition, which is in experiment $Mn_{1.22}Bi$ [90,91]. There is thus an excess of Mn in the sample. To examine the changes caused by the excess of Mn we performed test calculations for a hypothetical Mn_2Bi compound in the Heusler C_{1b} structure (i.e., MnMnBi), where each Mn atom is tetragonally surrounded by Bi. In the (111) direction this compound has a trigonal symmetry, like the (0001) NiAs phase. The calculated Kerr spectra of Mn_2Bi are also shown in Fig. 12 (dotted curve). In its Kerr rotation there is a peak at about 4.3 eV and a smaller one at 2 eV, which is at the same position as the main peak of MnBi. As Mn_2Bi in this structure is only a hypothetical compound, we have used a guessed lattice constant. The position of the peak at about 4 eV is rather sensitive to the lattice constant value. Thus, if the stoichiometry shifts from MnBi to Mn_2Bi there appears to be a tendency to reduce the first peak at 1.8 eV and to enhance the peak at about 3.5 eV. This corresponds exactly to what is seen

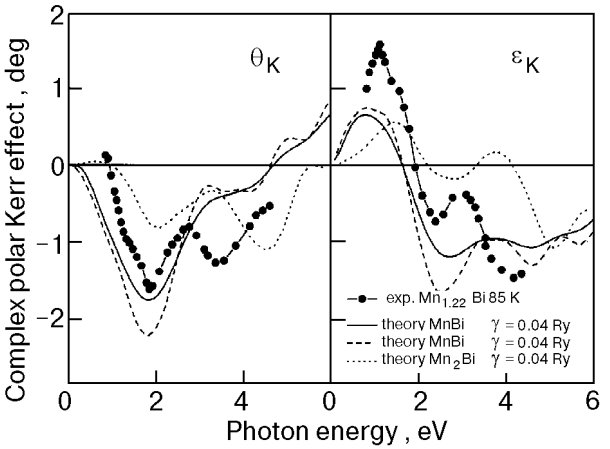

Fig. 12. Calculated and experimental Kerr spectra of Mn–Bi compounds. The Kerr rotation is denoted by θ_K , and the Kerr ellipticity by ε_K . The theoretical spectra are calculated for MnBi in the NiAs structure, for two lifetime broadenings, and for hypothetical Mn_2Bi in the Heusler C_{1b} structure. The experimental Kerr spectra were measured at 85 K on a $Mn_{1.22}Bi$ film [90].

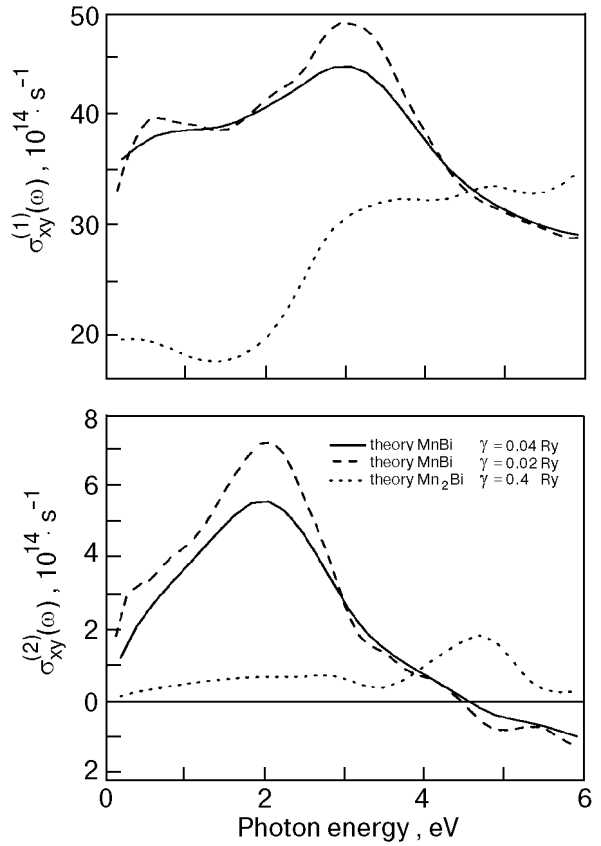

Fig. 13. Calculated absorptive parts of the optical conductivity, $\sigma_{xx}^{(1)}$ and $\sigma_{xy}^{(2)}$, for MnBi and Mn_2Bi.

in the experimental Kerr spectrum of composition $Mn_{1.22}Bi$. Other recent experiments on MnBi samples with an almost 2:1 Mn-Bi ratio confirm the trend of an increased Kerr rotation above 3 eV [92].

A further feature of the experimental Kerr rotation is that it exhibits a sign reversal at 0.9 eV. This sign reversal is actually also given by theory, but only for a smaller broadening parameter. This is consistent with the observation that experimentally it disappears in the room-temperature Kerr rotation [90,93]. Lastly, we mention that there appears to be a substantial intraband contribution to the conductivity present in the sample. In the calculations shown in Fig. 12 we accounted for the intraband conductivity by adding a Drude-type conductivity to the calculated interband conductivity. For this Drude conductivity we used the calculated plasma frequency and an estimated Drude broadening parameter (which is $\omega_p = 0.26$ Ry and $\gamma_D = 0.02$ Ry for MnBi). But, as adding a Drude conductivity shifts especially the Kerr ellipticity below 3 eV upwards, we would judge that in the sample there is likely a larger intraband contribution to the conductivity. This can be due to some disorder and the Mn-Bi stoichiometry.

The Kerr spectra depend on the MO conductivity spectra in an entangled way, so that it is difficult to assign features in the Kerr spectra to particular band transitions. The absorptive parts of the optical conductivity, $\sigma_{xx}^{(1)}$ and $\sigma_{xy}^{(2)}$, however, relate directly to the interband optical transitions, and provide therefore more physical insight. These absorptive parts of the conductivity tensor are shown for MnBi and Mn_2Bi in Fig. 13. The main peak in the Kerr rotation of MnBi is due to the maximum in $\sigma_{xy}^{(2)}(\omega)$ at 2 eV. Several kinds of dipolar optical transitions contribute to the broad structure in $\sigma_{xx}^{(1)}$. The main contributions originate from p–d and d–p transitions. The peak in $\sigma_{xy}^{(2)}$ is, however, mainly due to transitions from Bi p-like states.

As a first result, we conclude that first-principles electronic structure calculations give a satisfactory description of the giant Kerr rotation in MnBi. The difference between the experimental and *ab initio* Kerr rotation at 3.4 eV is anticipated to be related to the stoichiometry of the sample.

From these investigations the following picture of the Kerr effect in MnBi emerges: manganese has the required big magnetic moment of $3.71\mu_B$, while Bi has a small induced moment of $-0.10\mu_B$. In an applied field the small moment on Bi shifts to Mn (with sign reversed), so that then the total calculated moment compares well with the moment obtained from the saturation magnetization of

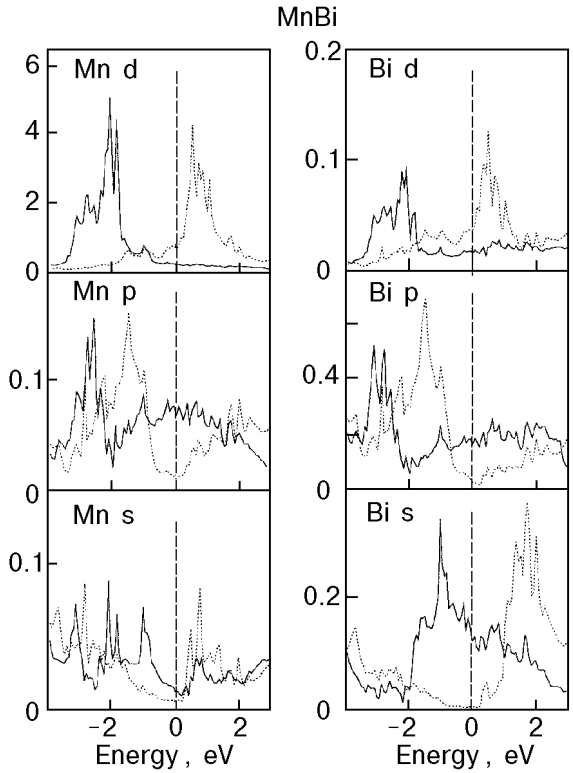

Fig. 14. Partial densities of states for MnBi, in units of states/(atom·eV).

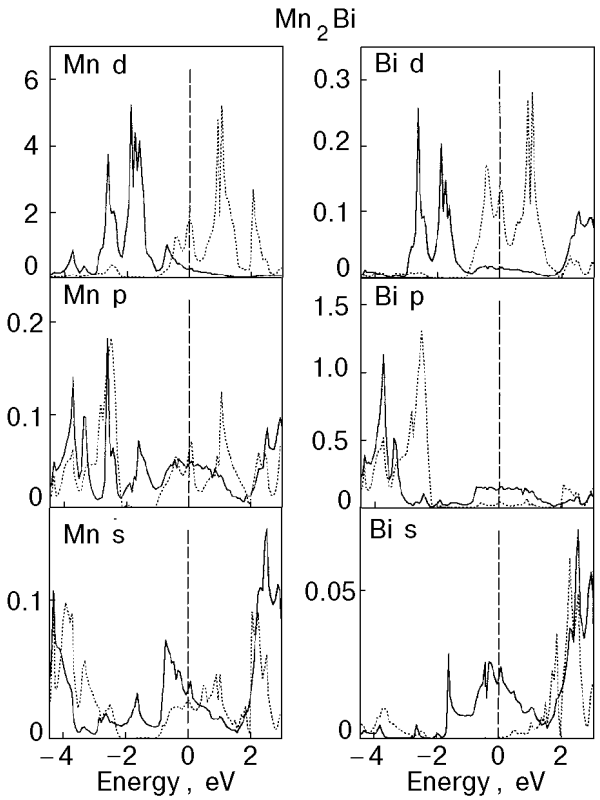

Fig. 15. As Fig.14, but for Mn_2Bi.

$(3.84 \pm 0.03)\mu_B$ [94]. Thus, in the interplay of exchange splitting and spin-orbit coupling leading to the record Kerr effect, Mn brings in the exchange splitting and Bi the spin-orbit coupling. The degree of hybridization between Mn and Bi, furthermore, can be recognized from the partial densities of states, which are shown in Fig. 14. There is a strong hybridization between the Bi and Mn *p*-type states as well as Bi and Mn *d*-type states, as can be seen from the identical shape of the partial densities. The magneto-optically active transitions take place mainly on Bi, from occupied *p*- to unoccupied *d*-states, in the spin-down bands (dotted curves). It is worth while to consider also the partial densities of states of Mn_2Bi, which are shown in Fig. 15. For this compound the Bi *p*-states are shifted down and are higher in density, and the hybridization is also large. As a result, the Kerr rotation at 4 eV becomes bigger. In contrast to MnBi, Mn_2Bi has its Fermi energy right at a maximum in the partial density of states, which suggests that this hypothetical compound will be unstable.

3. Localized *f* electrons: The case of CeSb and CeBi

Rare-earth compounds and alloys exhibit a great variety of unusual properties. Among them one finds heavy-fermion systems, intermediate valence compounds, Kondo metals, and Kondo insulators. To understand the physical properties of these materials correctly, it is necessary to investigate their electronic structure in detail. In this light, optical and MO spectroscopy has proven to be an extremely useful tool for the study of the *f* states in rare-earth and actinide compounds [4]. Over last decade the MO properties of rare earth compounds have attracted large interest [4], which increased after the discovery of the maximal observable rotation of 90° in CeSb by Pittini et al. [96]. The majority of MO investigations deal with compounds and alloys of the light rare earth ions Ce^{3+} and Nd^{3+}, the half-filled shell ion Eu^{2+} and the heavy rare earths Tm^{2+} and Yb^{3+}. As with most lanthanides, cerium and neodymium form face centered cubic (FCC) rock-salt type binary chalcogenides with the VIA elements of the periodic table of the elements (S, Se, Te) and FCC pnictides with the VA elements (N, P, As, Sb, Bi) [95]. With the exception of the nitrides, all cerium and neodymium chalcogenides and pnictides order antiferromagnetically in zero magnetic field. CeN is disordered down to 1.5 K, while NdN orders ferromagnetically [4]. The MO properties of cerium chalcogenides are well investigated experimentally [4,96,97], and also theoretically [15,31,33].

For CeSb a record Kerr angle of 90° was very recently reported [96], 90° is the absolute maximum value that can be measured. It is two orders of magnitude larger than the values that are commonly measured for transition-metal compounds, and about one order of magnitude larger than values maximally achieved for other lanthanide and actinide compounds [4]. To investigate the nature of a record polar Kerr rotation in CeSb, we have performed *ab initio* calculations of the optical spectra using the LDA and LDA+U approaches, with U = = 6 eV [33]. In Fig. 16 we show theoretical and experimental results for the real part of σ_{xx} for CeSb, CeTe and CeSe. From Fig. 16 it can be seen that for CeSe and CeTe the inclusion of the Coulomb interaction U leads to a substantial improvement over the LDA result. The erroneous peak at 1.5 eV in the LDA spectra, which is due to an unphysical $4f$ band resonance near E_F , dissapears in LDA+U spectra. Due to the Coulomb correlation, the occupied $4f^1$-levels are placed about 3–4 eV below E_F . In Fig. 17 we show the experimental [98] and LDA+U results for Kerr spectra of CeSe and CeTe. The results of the LDA approach are not shown here, but we mention that these do not by far reproduce the experimental data as good as LDA+U approaches [33]. The main peak in the Kerr rotation

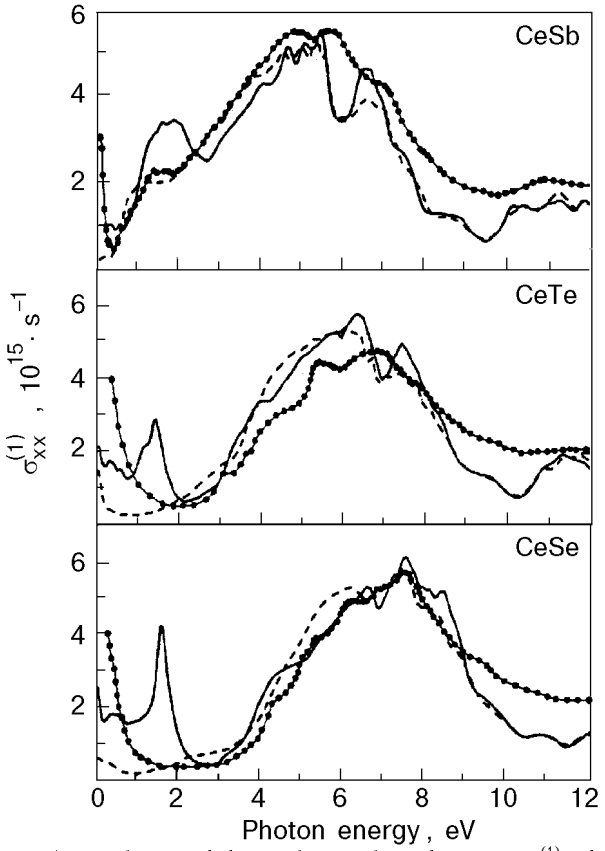

Fig. 16. Real part of diagonal optical conductivity, $\sigma_{xx}^{(1)}$, for CeSb, CeSe and CeTe. LDA results are depicted by the solid curves, LDA+U results by the dashed curves, and experimental results [98] are depicted by the solid dots.

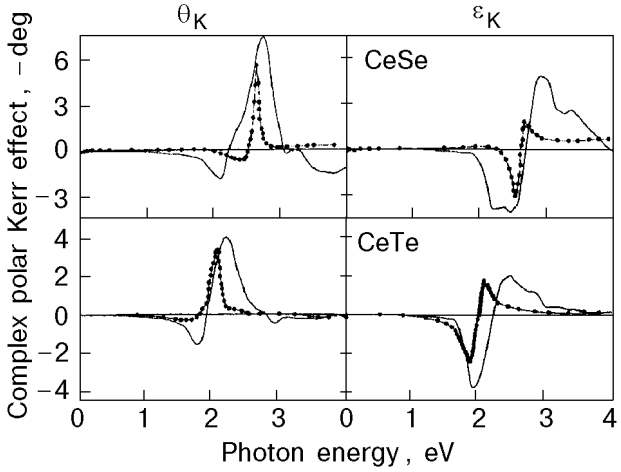

Fig. 17. Theoretical and experimental [98] Kerr angle (θ_K) and Kerr ellipticity (ε_K) spectrum of CeSe and CeTe. The theoretical spectrum (solid curve) was calculated using the LDA+U approach with U = 6 eV.

spectra in Fig. 17 is not found to be due to optical transitions stemming directly from the nearly localized $4f^1$-level. Instead, these peaks are due to a plasma minimum in the denominator of Eq. (3) and non-zero σ_{xy}, as will be discussed for CeSb below.

The LDA+U results for the Kerr spectra of CeSb are shown in Fig. 18. There is a giant Kerr rotation of 60° which is less than the observed value of 90°. Pittini et al. [96] observed that the maximum Kerr rotation depended on the magnetization and that therefore the intrinsic quantum state played an important role. In addition, the record Kerr effect occurs close to a plasma minimum. Both observations agree with what we find in our calculations. The denominator of Eq. (3) nearly vanishes due to the particular frequency dependence of σ_{xx}. A small denominator is not sufficient for obtaining a large Kerr rotation. Also σ_{xy}, which relates to the magnetic polarization, is important. The $4f^1$-level in CeSb is a completely spin and orbitally polarized state, which has a large magnetic moment of about $2\mu_B$. The $4f^1$-level is, however, located 3.6 eV beneath E_F in our calculations, and therefore it cannot contribute directly to the peak rotation. We find that the $4f^1$-level plays nevertheless a crucial role, because, due to hybridization of valence states with the anisotropically polarized $4f^1$-state, the valence bands become anisotropically polarized, This anisotropic polarization leads to an asymmetrical coupling of the left- and right-hand circularly polarized light at small photon energies. The asymmetrical light coupling leads in turn to a relatively large σ_{xy}, which causes the huge Kerr rotation. To emphasize the importance of the anisotropic hybridization, we also performed quasi-core calculations for the $4f^1$-level. We obtained a very similar

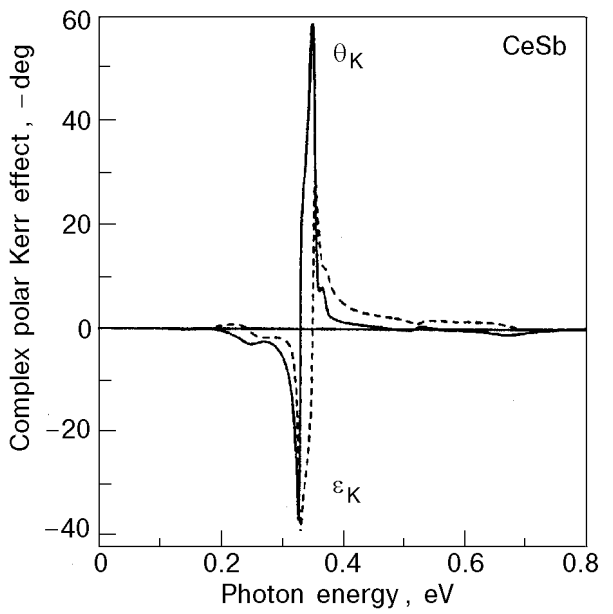

Fig. 18. Theoretical Kerr spectra of CeSb as calculated with LDA+U approach with U = 6 eV.

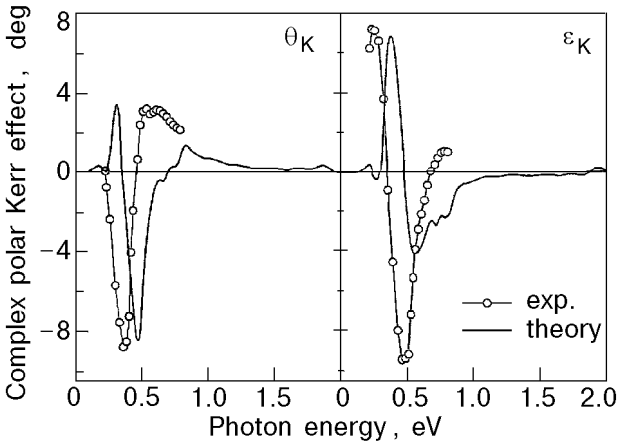

Fig. 19. Theoretical and experimental [98] Kerr angle (θ_K) and Kerr ellipticity (ε_K) spectrum of CeBi. The theoretical spectrum (solid curve) was calculated using the LDA+U approach with $U = 6$ eV.

σ_{xx} , but due to the lack of anisotropic 4*f*-hybridization, σ_{xy} becomes nearly zero. Consequently, only a very small Kerr rotation is obtained in quasi-core calculations.

The MO Kerr spectrum of CeBi has also a considerable interest. In most compounds the magnitude of the Kerr effect is proportional to the spin-orbit (SO) coupling interaction. The MO Kerr effect in MnBi is, for example, larger than that in MnSb, because the SO coupling on Bi is larger than that on Sb [24]. One could thus expect that the Kerr angle in CeBi should be as large as, or even larger, than that of CeSb. However, this is not found to be the case [98]. In Fig. 19 we show the experimental [98] and theoretical Kerr spectra of CeBi. The measured maximal Kerr rotation amounts only to −9°, ten times less than that of CeSb. The LDA+U approach (with $U = 6$ eV) explains the measured MO Kerr spectrum of CeBi fairly well. There is a small energy difference of 0.1 eV in the position of the rotation maximum, and the calculated Kerr ellipticity deviates above 0.5 eV from the experimental curve.

The fact that the Kerr rotation of CeBi is far less that that of CeSb is fully reproduced by our calculations [28,33], but it is not consistent with our experience that the Kerr effect is proportional to the magnitude of SO coupling. The imaginary part of σ_{xy} is for CeBi as large as that of CeSb, but if we compare the σ_{xx} of CeBi to that of CeSb, then we find that the denominator does not become as small for CeBi. The resulting Kerr angle of CeBi is therefore not as large as that of CeSb.

We conclude that LDA+U approach provides an improved electronic structure for materials having deep-lying, nearly localized *f*'s. The optical and MO spectra computed therefrom are in fair accord with experimental spectra. The overall agreement of the calculated and experimental spectra, however, emphasizes that improvements are still called for.

4. Uranium compounds

Intensive experimental and theoretical study over more than two decades [99–103] has revealed that 5*f* magnetism is quite complex, because Coulomb, spin-orbit, crystalline field and exchange energies in 5*f* systems are the same order of magnitude. Today it is well established that many unusual physical properties of the light actinide metals are a reflection of the particular nature of the 5*f* electrons. Many years ago Friedel [104] proposed that the bonding in these materials must involve the 5*f* electrons. The argument for 5*f* bonding can be understood as a consequence of the extended nature of the 5*f* wave function relative to the rare-earth 4*f* wave functions. This causes them to form in band-like states [105].

The itinerant nature of the 5*f* electrons in the light actinide metals are well known [99]. Their electronic structure and optical properties are well described by LDA band structure calculations [106,107]. On the other hand, the decreasing *f*-band width (W) and the increasing intraatomic Coulomb energy (U) results in a Mott localization in between plutonium and americium [100,108,109] and the correlation effects are not properly described in the local density approximation [102,110].

Actinide compounds occupy an intermediate position between itinerant 3*d* and localized 4*f* systems [111,112] and one of the fundamental questions concerning the actinide materials is whether their *f* states are localized or itinerant. This question is most frequently answered by comparison between experimental spectroscopies and the different theoretical descriptions.

Optical spectroscopy provides a powerful, widely used tool to investigate in detail the electronic structure of actinides. Traditionally, one distinguishes the various existing kinds of spectroscopies according to the photon energy of the employed light, i.e., high-energy x-ray methods, and methods applying infrared, visible or medium-energy light ($\hbar\omega < 10$ eV). X-ray photoemission spectroscopy (XPS) has been applied to determine the energy position of the 5*f* states below E_F , and angle-resolved XPS has been used to map out the energy bands in the Brillouin zone (see, e.g.,[113]). Optical spectroscopy in the visible and infrared energy range has successfully been applied to many topics

in the actinide research. Examples are the infrared absorption in the heavy-fermion state of URu_2Si_2 [114] and UPd_2Al_3 [115], reflectivity spectroscopy on intermediate valence and dense Kondo materials [116]. A particular useful spectroscopic technique is MO Kerr spectroscopy [4]. Reflectivity spectroscopy can be used to determine relative energy level positions, but Kerr spectroscopy has the additional advantage that it couples to both the spin and orbital polarization of the electron states [4]. Kerr spectroscopy is therefore ideally suited for studying magnetic actinide compounds. On the other hand, actinide compounds are also excellent subjects for MO research. The participation of the $5f$ states in bonding is reflected in strongly hybridized bands near the Fermi level, with a high density of states and significant $f \to d$ oscillator strengths for optical transitions. The $5f$ delocalization favors higher ordering temperatures. In fact, many uranium compounds have ordering temperatures which are one order of magnitude larger than those in similar lanthanide compounds [4,117]. Regarding the magnitude of the MO effects compared to rare-earth materials, an enhancement due to the larger spin-orbit energy can be expected and is in part experimentally verified [4,117]. For actinide compounds the figure of merit $R^{1/2}(\theta_K^2 + \varepsilon_K^2)^{1/2}$, where R is the optical reflectivity, θ_K and ε_K are Kerr angle and Kerr ellipticity, respectively, is one order of magnitude larger than for the best transition or rare-earth compounds [4]. Besides the issue of radioactivity (minimal for depleted uranium) a hindrance for successful application of actinide compounds in storage devices is that the typical Curie temperature are below room temperature. This is not a fundamental problem, and can probably be overcome by suitable alloying.

As we mentioned above one of the most intriguing aspects of actinide compounds is the great variability in the localization degree of the $5f$ electrons. Varying from one actinide compound to another, the $5f$ electrons may range from being nearly localized to being practically itinerant. In this work we consider two groups of actinide compounds. The optical and MO spectra of the first group which contains UAsSe and URhAl compounds can be properly described within density functional theory in the local-density approximation, but such an approximation totally failed in the case US, USe, and UTe. This result puts forward further evidence for at least partly itinerant electron behavior in the first group compounds and at least partly localized one in the second group.

4.1. UAsSe *and* URhAl

UAsSe crystallizes in the tetragonal PbFCl crystal structure (also called ZrSiS structure, P4/nmm space group) and orders ferromagnetically below $T_C \approx 110$ K [118,119]. Magnetic susceptibility measurements [120] and photo-emission experiments [121] supplied evidence for localized $5f$ electrons in UAsSe. On the other hand, reflectivity and MO spectroscopy revealed a pronounced spectral intensity at small photon energies (< 2 eV) which was attributed to a $5f$ band located at the Fermi energy [117]. Also, the specific heat coefficient $\gamma = 41$ mJ/mol·K^2 indicates a tendency to itinerancy [122]. These apparently contradicting observations show that the behavior of the $5f$ electrons and the related magnetic properties of UAsSe are not yet well understood.

As in other uranium compounds with non-cubic structures such as, e.g., the ternary UT_2X_2 compounds [123] there is the possibility of partially delocalized electrons in another sense. These compounds with a preferred c-axis tend to have the uranium atoms arranged in layers which leads to both anisotropic bonding and magnetic properties due to hybridization of $5f$ and p or d states. It is quite possible that the $5f$ electrons are delocalized in the planes but localized along the c-axis and we suspect that this may be the case in UAsSe. In this compound the uranium planes are perpendicular to the axis of the polar Kerr measurements, so that the polar MO Kerr effect selectively probes these planes which is a possible explanation [5] of why the response appears to be due to itinerant electrons.

A comparison of the theoretical and experimental spectra in Fig. 20 proves that there is a very good agreement between the band theory and experimental data: Both the position and height of the main peak in the Kerr angle (θ_K) at 3 eV are properly

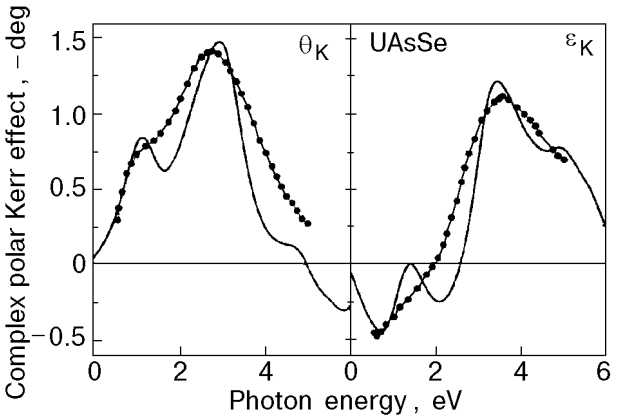

Fig. 20. Theoretical and experimental polar Kerr rotation and Kerr ellipticity spectra of UAsSe. The experimental data (■) are after Reim (Ref. 5).

given by theory, with the usual (small) dependence of the theoretical peak height on the broadening. Energy-band theory predicts also a smaller peak in the Kerr rotation at 1 eV, where there is only a shoulder seen in the measured Kerr angle. A Kramers-Kronig related peak structure is visible in the Kerr ellipticity (ε_K) spectrum at 1.5 eV. In this energy region there will of course be the influence of the not included intraband conductivity which may change the pure interband spectra.

URhAl has also a layer crystal structure with U-Rh planes separated by Rh-Al planes. There are apparently several contradicting experimental observations on the nature of $5f$-electron localization in URhAl. Inelastic neutron scattering experiments on URhAl revealed a peak at 380 meV, which could be the signature of an intermultiplet transition [124]. The value of 380 meV is quite close to the intermultiplet transition energy of 390 meV measured for UPd_3 [125]. There are, however, several other properties of URhAl that would advocate rather delocalized $5f$ behavior in URhAl. A small U moment of only $0.94\mu_B$ was measured which does corresponds to the magnetic moment of neither a $5f^2$ nor a $5f^3$ configuration [126]. A significant amount of anisotropic $5f$-ligand hybridization was reported [127]. Also, the measured specific heat $\gamma = 60$ mJ·mol^{-1}·K^{-2} is not particularly small [128]. These contradictory observations demonstrate that the $5f$ behavior in URhAl is not yet understood.

In Fig. 21 we show the experimental Kerr spectrum [129] of URhAl together with the theoretical spectrum calculated using the itinerant LDA approach [28]. The first spectral peak at 1 eV, and the second one at 2–3 eV in the Kerr angle are definitely reproduced in the theoretical spectrum. The theoretical Kerr rotation drops off between 4 and

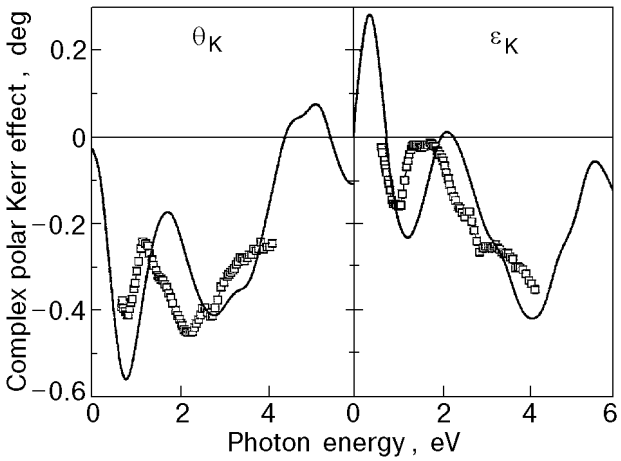

Fig. 21. Experimental [129] and theoretical Kerr spectrum of URhAl. The theoretical spectrum is calculated with the itinerant LDA approach.

5 eV, but it is yet not clear if this also occurs in the experimental θ_K spectrum. It can, nevertheless, be concluded that the itinerant $5f$ model explains the measured Kerr spectrum fairly well. Clearly, this supports the picture of delocalized $5f$ electrons in URhAl. The calculated electronic specific heat coefficient, $\gamma = 41$ mJ·mol^{-1}·K^{-2}, is quite reasonable since a many-body enhancement of 1.5 can be considered to be normal.

With respect to the signified intermultiplet transition, it could be speculated that the $5f$'s in URhAl divide into two groups, relatively delocalized, rather hybridized $5f$'s in the U-Rh plane, and more localized $5f$'s perpendicular to this plane, in accord with the observation of anisotropic f hybridization in URhAl [127]. The possible intermultiplet transition might correspond to the localized $5f$'s, whereas Kerr spectroscopy in the polar geometry probes the MO response in the U-Rh plane.

In conclusion, we find that the MO Kerr spectra of UAsSe and URhAl can be excellently described by a LDA band-structure approach to the $5f$ electrons.

4.2. US, USe and UTe

The uranium compounds US, USe, and UTe belong to the class of uranium monochalcogenides that crystallize in the NaCl structure and order ferromagnetically (on the uranium sublattice) at Curie temperatures of 178, 160, and 102 K, respectively (see, e.g., the review [130]). These uranium compounds exhibit several unusual physical phenomena, which are the reason for an as yet ongoing interest in these compounds. Despite their relatively simple and highly symmetrical NaCl structure, it has been found that the magnetic ordering on the uranium atoms is strongly anisotropic [131,132], with the uranium moment favoring a (111) alignment. The magnetic anisotropy in US, e.g., is one of the largest measured in a cubic material, with a magnetic anisotropy constant K_1 of more than 2×10^8 erg/cm^3 [133]. Also the magnetic moment in itself is unusual, consisting of an orbital moment that is about twice as large as the spin moment, and of opposite sign [134–136], but it is not close to the atomic moment. In addition to this, these materials show with increasing mass of the chalcogenide atom evidence of correlated-electron behavior, with UTe being considered as a dense Kondo system [137]. Obviously, the uranium $5f$-electrons are to be held responsible for both features.

Schoenes and Reim [4,77,117,138,139,] investigated the magneto-optical (MO) spectra of these

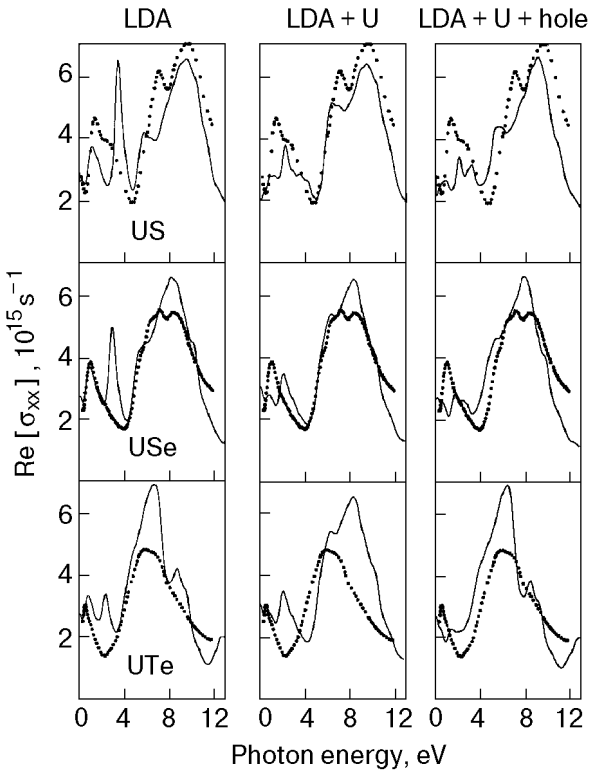

Fig. 22. Real part of diagonal optical conductivity, $\sigma_{xx}^{(1)}$, for US, USe and UTe in LDA, LDA+U approximations and with a screened hole in the $5f^2$-shell (LDA+U+hole) Theoretical results are depicted by the solid curves, and experimental results [4] are depicted by the solid dots.

uranium salts and obtained three rather similar Kerr spectra, as one would expect from isochemical compounds. Besides, the measured Kerr rotation spectra are unusually large, with peak values of about 3 degrees. In a first interpretation of their measurements Reim and Schoenes gave an analysis of the Kerr spectra in terms of optical transitions on uranium [117,139].

It has already been shown that first-principles band-structure theory using the local density approximation has failed in giving a satisfactory description of the optical spectra of the uranium monochalcogenides [4,77]. This failure was thought to be due to an insufficient treatment of the *f*-electron correlations by the LDA [4]. These many-body correlation effects can already be important for the proper description of ground state properties, but they should become imperative for describing optical excitations. For example, if a strong on-site Coulomb repulsion between electron and hole quasiparticles plays a dominating role [140]. Therefore, if the uranium $5f$ electrons are localized, then one would particularly expect to observe corresponding electron correlation effects in the optical spectra. The behavior of the $5f$ electrons ranges from nearly delocalized to almost localized: US is considered to be nearly itinerant [141], while UTe is considered to be quasilocalized [142]. So the failure of LDA discription of MO Kerr spectra in US comes as a surprise, because, if the $5f$-electrons are itinerant, one would expect the delocalized LDA approach to be applicable.

To find the appropriate description, we carried out various model calculations of the optical and MO spectra [20,22]. These included the orbital polarization [143] and the LDA+U approach, assuming $5f^2$ and $5f^3$ configurations for uranium (with $U = 2$ eV). However, using these approaches we could not obtain satisfactory agreement with the experimental spectra for all three compounds. In Fig. 22 we show theoretical and experimental results for the real part of $\sigma_{xx}^{(1)}$, for US, USe and UTe. From Fig. 22 it can be seen that for US and USe the inclusion of the Coulomb interaction U leads to a substantial improvement over LDA result. The erroneous peak at 3 eV in the LDA spectra disappears in LDA+U spectra. In Fig. 23 we show theoretical and experimental results for the imaginary part of offdiagonal part of optical conductivity $\sigma_{xy}^{(2)}$, for US, USe and UTe. It can be seen that LDA calculations gives completely inappropriate results. LDA+U calculations are greatly improve the agreement between theory and experiment in the case of USe and UTe. This finding appears to be consistent

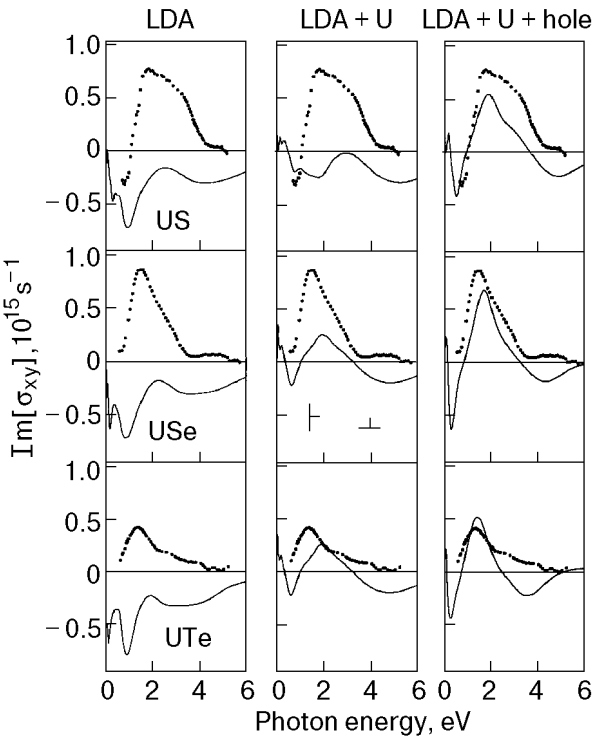

Fig. 23. As Fig. 22, but for imaginary part of offdiagonal optical conductivity, $\sigma_{xy}^{(2)}$.

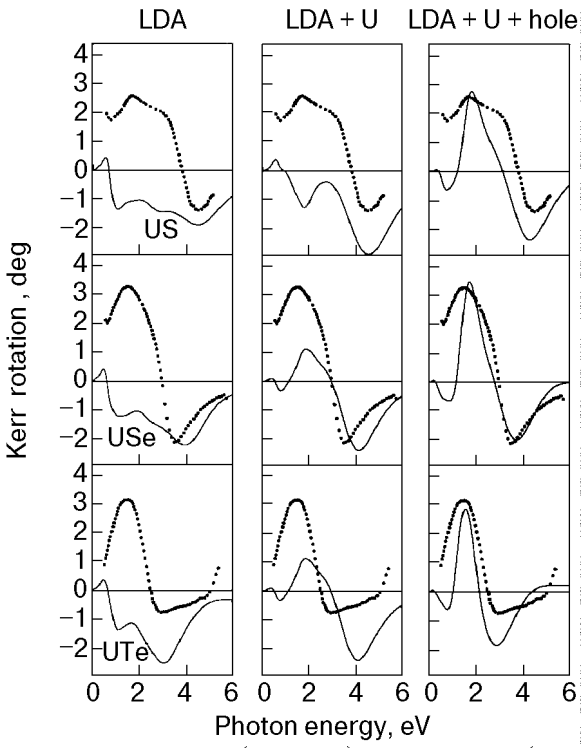

Fig. 24. Experimental [4] (solid dots) and theoretical (solid line) Kerr spectra of US, USe and UTe.

with the quasilocalized nature of the 5*f*-electrons in USe and UTe. As for US, the dynamical process of the optical excitations may provide a clue for understanding what happens: the photoemission of a 5*f*-electron creates a long-living hole in the 5*f*-shell, which will be rapidly screened. This hole in the broad, semilocalized 5*f*-bands lies in the important spectral range. To test the influence of this process we performed LDA+U calculations (with $U = 2$ eV) and with a screened hole in the $5f^2$-shell. The physically motivated correction leads to an improved description of the optical conductivity (see Figs. 22 and 23) and also Kerr spectrum for US, USe and UTe (Fig.24).

Summary

Recent progress in first-principle calculations of optical spectra illustrates that optical and MO spectra are developing into a powerful tool for tracing the electronic structure of crystals. The density-functional theory in the local-density approximation gives a fully satisfactory explanation of the MO Kerr spectra of transition metal compounds and alloys in most cases. Moreover, theory can help to understand the nature of MO spectra and gives some recommendations how to create compounds with appropriate MO properties.

As can be seen from the consideration of MO properties of MnBi, XPt_3 compounds and Heusler alloys, large Kerr effects can be anticipated when compounds fulfill the following conditions: one of the constituting elements must be heavy, but this element need not be magnetic, for instance, Pt or Bi. One of the other elements must have a large moment, but this element need not be heavy, for instance, Mn, Fe or Co. In addition should there be a good hybridization between the states of the two kinds of atoms. Within such a composition, the large exchange splitting (i.e., a big magnetic moment) and the strong spin-orbit coupling lead through the hybridized bands to a big Kerr rotation. However, not in all cases does this «rule of thumb» apply, because sometimes the influence of the band structure can be such that dipolar transitions of different bands compensate each other.

In most of the 4*f* systems, the *f* electrons are localized and form a Hund's rule ground state. The application of plain LDA calculations to 4*f* electron systems encounters problems in most cases, because of the correlated nature of electrons in the *f* shell. To better account for strong on-site electron correlations the LDA+U approach should be used, in which a model Hamiltonian explicitly including the on-site Coulomb interaction, U, for localized states is combined with the standard band structure calculation Hamiltonian for extended states. The LDA+U method provides a rather good description of the electronic structure and the optical and MO properties of some lanthanide compounds [20,28,32].

Actinide compounds occupy an intermediate position between itinerant 3*d* and localized 4*f* systems, and one of the fundamental questions concerning the actinide materials is whether their *f* states are localized or itinerant. This question is most frequently answered by comparison between experimental spectroscopies and the different theoretical descriptions. Optical and MO spectroscopy, like photoelectrons spectroscopy and bremsstrahlung isochromat spectroscopy supply direct information about the energy states (both occupied and unoccupied) around the Fermi energy, and can provide a means of discrimination between the two theoretical limits.

There are quite a few first-principle calculations of the MO spectra of uranium compounds [9,19,20, 22,144]. The MO spectra of such compounds as UAsSe [19], URhAl [28], U_3P_4 [144,145] and U_3As_4 [145] are well described in the LDA and we can conclude that they have at least partially itinerant electron behavior. On the other hand, the MO spectra in UTe can be well described only in the LDA+U approximation [20] supporting the localized description for their 5*f* electrons. The most

difficult case is US which is commonly classified to be itinerant. We find that a LDA+U approach supplemented with a screened hole in the 5*f*-shell gives a reasonable description of the Kerr spectra of US and USe.

Acknowledgments

We thank Dr. S. Iwata for sending us the Kerr spectra of $MnPt_3$.

We are indebted to Prof. Katsuaki Sato and Dr. Koki Takanashi for informing us about MO investigations of PtMnSb and related materials.

We thank Dr. S. Iwata and Dr. G. Q. Di for sending us their measured MnBi spectra, and thank Prof. Y. J. Wang for informing us about recent results. Further we thank Dr. G. Q. Di for correcting the MnBi Kerr spectra for the influence of the quartz refractive indices.

We thank Prof. J. Schoenes, M. S. S. Brooks, and O. Eriksson for valuable discussions and comments.

1. J. Kerr, *Phil. Mag.* **3**, 321 (1877).
2. C. D. Mee and E. D. Daniel, *Magnetic Recording*, McGraw-Hill, New York (1987); M. Mansuripur, *The Physical Prmciples of Magneto-Optical Recording*, University Press, Cambridge (1995).
3. K. H. J. Buschow, in: *Ferromagnetic Materials*, E. P. Wohlfarth and K. H. J. Buschow (eds.), North-Holland, Amsterdam (1988), Vol. 4, p. 588.
4. W. Reim and J. Schoenes, in: *Ferromagnetic Materials*, E. P. Wohlfarth and K. H. J. Buschow (eds.), North-Holland, Amsterdam (1990), Vol. 5, p. 133.
5. J. Schoenes, in: *Materials Science and Technology*, Vol. 3A: *Electronic and Magnetic Properties of Metals and Ceramics*, K. H. J. Buschow, R. W. Cahn, P. Hassen and E. J. Kramer (eds.), Verlag Chemic, Weinheim (1992), p. 147.
6. H. R. Hulme, *Proc. Roy. Soc.* **A135**, 237 (1932).
7. C. Kittel, *Phys. Rev.* **83**, A208 (1951).
8. P. N. Argyres, *Phys. Rev.* **97**, 334 (1955).
9. B. R. Cooper, *Phys. Rev.* **139**, A1504 (1965).
10. G. S. Krinchik and E. A. Gan'sbina, *Zh. Eksp. Teor. Fiz.* **65**, 1970 (1913) [*Sov. Phys. JETP* **38**, 983 (1974)].
11. R. Kubo, *J. Phys. Soc. Jpn.* **12**, 570 (1957).
12. A. E. Kondorsky and A. V. Vediaev, *J. Appl. Phys.* **39**, 559 (1968).
13. C. S. Wang and J. Callaway, *Phys. Rev.* **B9**, 4897 (1974).
14. G. H. O. Daalderop, F. M. Mueller, R. C. Albers, and A. M. Boring, *J. Magn. Magn. Mat.* **74**, 211 (1988); H. Ebert, P. Strange, and B. L. Gyorffy, *J. Phys.* **CS**, 31 (1988); Yu. Uspenskii and S. V. Halilov, *Zh. Eksp. Teor. Fiz.* **95**, 1022 (1989) [*Sov. Phys. JETP* **68**, 588 (1989).
15. E. T. Kulatov, Yu. A. Uspenskii, and S. V. Khalilov, *Phys. Lett.* **A195**, 267 (1994); Yu. A. Uspenskii, E. T. Kulatov, and S. V. Khalilov, *Zh Eksp. Teor. Fiz.* **1**, 1708 (1995) [*Phys. JETP* **80**, 952 (1995)]; Ya. A. Uspenskii, E. T. Kulatov, and S. V. Khalilov, *Phys. Rev.* **B54**, 474 (1996); E. T. Kulatov, Yu. A. Uspenski, and S. V. Khalilov, *Fiz. Tverd. Tela* **38**, 3066 (1970) [*Sov. Phys. Solid State* **38**, 1677 (1996).
16. P. M. Oppeneer, J. Sticht, and F. Herman, *J. Magn. Soc. Jpn.* **15**, Sl, 73 (1991); P. M. Oppeneer, T. Maurer, J. Sticht, and J. Kübler, *Phys. Rev.* **B45**, 10924 (1992); I. Osterloch, P. M. Oppeneer, J. Sticht, and J. Kübler. *J. Phys. Cond. Mat.* **6**, 285 (1994); J. Kühler, L. Sandratskii, and J. Kübler, *Physica* **B253**, 272 (1998).
17. V. N. Antonov, A. Ya. Perlov, A. P. Shpak, and A. N. Yaresko, *J. Magn. Magn. Mater.* **146**, 205 (1995).
18. P. M. Oppeneer and V. N. Antonov, in: *Spin-Orbit Influenced Spectroscopies of Magnetic Solids*, H. Ebert and G. Schiitz (eds.), Springer, Berlin (1996), p. 29.
19. P. M. Oppeneer, M. S. S. Brooks, V. N. Antonov, T. Kraft, and H. Eschrig, *Phys. Rev.* **B53**, R10437 (1996).
20. P. M. Oppeneer, V. N. Antonov, A. Ya. Perlov, A. N. Yaresko, T. Kraft, and H. Eschrig, *Physica* **B230-232**, 544 (1997).
21. P. M. Oppeneer, V. N. Antonov, T. Kraft, H. Eschrig, A. N. Yaresko, and A. Ya. Perlov, *Solid State Commun.* **94**, 255 (1995).
22. T. Kraft, P. M. Oppeneer, V. N. Antonov, and H. Eschrig, *Phys. Rev.* **B52**, 3561 (1995).
23. P. M. Oppeneer, V. N. Antonov, A. N. Yaresko, A. Ya. Perlov, T. Kraf, and H. Eschrig, *J. Magn. Soc. Jpn.* **20**, *Suppl.* Sl, 41 (1996).
24. P. M. Oppeneer, V. N. Antonov, T. Kraf, H. Eschrig, A. N. Yaresko, and A. Ya. Perlov, *J. Appl. Phys.* **80**, 1099 (1996).
25. P. M. Oppeneer, V. N. Antonov, T. Kraf, H. Eschrig, A. N. Yaresko, and A. Ya. Perlov, *J. Phys. Condens. Matter* **8**, 5769 (1996).
26. V. N. Antonov, P. M. Oppeneer, A. N. Yaresko, A. Ya. Perlov, and T. Kraft, *Phys. Rev.* **B56**, 13012 (1997).
27. A. Ya. Perlov, H. Ebert, A. N. Yaresko, V. N. Antonov, and D. Weller, *Solid State Commun.* **105**, 273 (1998).
28. P. M. Oppeneer, A. Ya. Perlov, V. N. Antonov, A. N. Yaresko, T. Kraft, and M. S. S. Brooks, *J. Alloys and Compounds* **271-273**, 831 (1998).
29. A. N. Yaresko, L. Uba, S. Uba, A. Ya. Perlov, R. Gontarz, and V. N. Antonov, *Phys. Rev.* **B58**, 5043 (1998).
30. S. P. Lim, D. L. Price, and B. R. Cooper, *IEEE Trans. Magn.* **27**, 3648 (1991); B. R. Cooper, S. F. Lim, and I. Avgin. *J. Phys. Chem. Solids* **56**, 1518 (1995).
31. X. Wang, V. P. Antropov, and B. N. Harmon, *IEEE Trans. Magn.* **30**, 4458 (1994); V. P. Antropov, A. I. Liechtenstein, and B. N. Harmon, *J. Magn. Magn. Mat.* **140**, 1161 (1995); B. N. Harmon, V. P. Antropov, A. I. Liechtenstein, I. V. Soloviev, and V. I. Anisimov. *J. Phys. Chem. Solids* **56**, 1521 (1995); Yu. A. Uspenskii, V. P. Antropov, and B. N. Harmon. *Phys. Rev.* **B56**, R11396 (1997).
32. A. I. Liechtenstein, V. P. Antropov, and B. N. Harmon, *Phys. Rev.* **B49**, 10770 (1995).
33. A. N. Yaresko, P. M. Oppeneer, A. Ya. Perlov, V. N. Antonov, T. Kraft, and H. Eschrig, *Europhys. Lett.* **36**, 551 (1996).
34. S. Uba, L. Uba, A. Ya. Perlov, A. N. Yaresko, V. N. Antonov, and R. Gontarz, *J. Phys.: Condens. Matter.* **9**, 447 (1997).
35. H. Ebert, A. Ya. Perlov, A. N. Yaresko, V. N. Antonov, and S. Uba, in: *Magnetic Ultrathin Films, Multilayers and Surfaces*, J. Tobin et al. (eds.), Pittsburg, Pensilvania (1997), p. 407.
36. S. Uba, L. Uba, R. Gontarz, V. N. Antonov, A. Ya. Perlov, and A. N. Yaresko, *J. Magn. Magn. Mater.* **140-144**, 575 (1995).

37. S. Uba, L. Uba, A. N. Yaresko, A. Ya. Perlov, V. N. Antonov, and R. Gontarz, *Phys. Rev.* **B53**, 6526 (1996).
38. S. Uba, A. N. Yaresko, L. Uba, A. Ya. Perlov, V. N. Antonov, and R. Gontarz, *Phys. Rev.* **B57**, 1534 (1997).
39. S. Uba, L. Uba, A. N. Yaresko, A. Ya. Perlov, V. N. Antonov, and R. Gontarz, *J. Phys.: Condens. Matter.* **10**, 7769 (1998).
40. R. Gontarz, S. Uba, L. Uba, A. Ya. Perlov, A. N. Yaresko, and V. N. Antonov, in: *Frontiers in Magnetism of Reduced Dimension Systems*, P. E. Wigen (ed.), *Proc. of NATO Advanced Research Workshops, ASI* — Kiev, Ukraine, 1997 KLUWER Academic Publishers, Netherlands (1998).
41. W. H. Kleiner, *Phys. Rev.* **142**, 318 (1966).
42. A. H. MacDonald and S. H. Vosko, *J. Phys. C: Solid State Phys.* **12**, 2977 (1979).
43. H. Ebert, H. Freyer, A. Vernes, and G. -Y. Guo, *Phys. Rev.* **B53**, 7721 (1996).
44. H. Ebert, *Phys. Rev.* **B38**, 9390 (1988).
45. I. V. Solovyev, A. B. Shik, V. P. Antropov, A. I. Liechtenstein, V. A. Gubanov, and O. K. Andersen, *Sov. Phys. Solid State* **31**,1285 (1989).
46. O. K. Andersen, *Phys. Rev.* **B12**, 3060 (1975).
47. V. V. Nemoshkalenko, A. E. Krasovskii, V. N. Antonov, Vl. N. Antonov, U. Fleck, H. Worm, and P. Ziesche, *Phys. Status Solidi* **B120**, 283 (1983).
48. A. Santoni and F. J. Himpsel, *Phys. Rev.* **B43**, 1305 (1991).
49. V. N. Antonov, A. I. Bagljuk, A. Ya. Perlov, V. V. Nemoshkalenko, Vl. N. Antonov, O. K. Andersen, and O. Jepsen, *Low Temp. Phys.* **19**, 494 (1993).
50. V. I. Anisimov, J. Zaanen, and O. K. Andersen, *Phys. Rev.* **B44**, 943 (1991).
51. P. W. Anderson, *Phys. Rev.* **124**, 41 (1961).
52. V. I. Anisimov, F. Aryasetiawan, and A. I. Liechtenstein. *J. Phys.: Condens. Matter.* **9**, 767 (1997).
53. P. M. Oppeneer, V. N. Antonov, A. N. Yaresko, A. Ya. Perlov, and H. Eschrig, *Phys. Rev. Lett.* **78**, 4079 (1997).
54. V. N. Antonov, A. N. Yaresko, A. Ya. Perlov, P. Thalmeier, P. Fulde, P. M. Oppeneer, and H. Eschrig, *Phys. Rev.* **B58**, 9752 (1998).
55. P. G. van Engen, K. H. J. Buschow, R. Jongebreur, and M. Erman, *Appl. Phys. Lett.* **42**, 202 (1983).
56. B. M. Lairson and B. M. Clemens, *Appl. Phys. Lett.* **63**, 1438 (1993).
57. G. R. Harp, D. Weller, T. A. Rabedeau, R. F. C. Farrow, and M. F. Toney, *Phys. Rev. Lett.* **71**, 2493 (1993).
58. W. B. Zeper, F. J. A. M. Greidanus, P. F. Garcia, and C. R. Fincher, *J. Appl. Phys.* **65**, 4971 (1989).
59. D. Weller, H. Brandle, G. Gorman, C. -J. Lin, and H. Notarys, *Appl. Phys. Lett.* **61**, 2726 (1992).
60. K. Sato, H. Ikedame, Y. Tosaka, K. Tsuzukiyama, Y. Togami, and M. Fujisawa, *J. Magn. Magn. Mater.* **126**, 572 (1993).
61. T. Kato, H. Kikuzawa, S. Iwata, S. Tsunashima, and S. Uchiyama, *J. Magn. Magn. Mater.* **140-144**, 713 (1995).
62. T. Kato, S. Iwata, S. Tsumashima, and S. Uchiyama, *J. Magn. Soc. Jpn.* **19**, 205 (1995).
63. P. G. van Engen, K. H. J. Buschow, and M. Erman, *J. Magn. Magn. Mater.* **30**, 374 (1983).
64. P. G. van Engen, *PhD thesis*, Technical University Delft, (1983).
65. R. A. de Groot, F. M. Mueller, P. G. van Engen, and K. H. J. Buschow, *Phys. Rev. Lett.* **50**, 2024 (1983).
66. K. E. H. M. Hanssen, P. E. Mijnarends, L. P. L. M. Rabou, and K. H. J. Buschow, *Phys. Rev.* **B42**, 1533 (1990).
67. E. Kisker, C. Carbone, C. F. Flipse, and E. F. Wassermann, *J. Magn. Magn. Mater.* **70**, 21 (1987).
68. G. L. Bona, F. Meier, M. Taborelli, E. Bucher, and P. H. Schmidt, *Solid State Commun.* **56**, 391 (1985).
69. J. S. Moodera and D. M. Mootoo, *J. Appl. Phys.* **76**, 6101 (1994).
70. J. F. Bobo, P. R. Johnson, M. Kautzky, F. B. Mancoff, E. Tuncel, R. L. White, and B. M. Clemens, *J. Appl. Phys.* **81**, 4164 (1997).
71. R. A. de Groot, F. M. Mueller, P. G. van Engen, and K. H. J. Buschow, *J. Appl. Phys.* **55**, 2151 (1984).
72. H. Feil and C. Haas, *Phys. Rev. Lett.* **58**, 65 (1987).
73. J. H. Wijngaard, C. Haas, and R. A. de Groot, *Phys. Rev.* **B40**, 9318 (1989).
74. G. Y. Guo and H. Ebert, *Phys. Rev.* **B50**, 10377 (1994).
75. G. Y. Guo and H. Ebert, *Phys. Rev.* **B51**, 12633 (1995).
76. K. J. Kim, T. C. Leung, B. N. Harmon, and D. W. Lynch, *J. Phys.: Condens. Matter.* **6**, 5069 (1994).
77. T. Gasche, *PhD thesis*, Uppsala (1993).
78. T. Gasche, M. S. S. Brooks, and B. Johansson, *Phys. Rev.* **B53**, 296 (1996).
79. N. Mainkar, D. A. Browne, and J. Callaway, *Phys. Rev.* **B53**, 3692 (1996).
80. S. Shiomi, A. Ito, and M. Masuda, *J. Magn. Soc. Jpn.* **11**, S1, 221 (1987).
81. M. C. Kautzky and B. M. Clemens, *Appl. Phys. Lett.* 66, 1279 (1995).
82. T. Inukai, N. Sugimoto, M. Matsuoka, and K. Ono, *Appl. Phys. Lett.* **49**, 52 (1986).
83. K. Takanashi, H. Fujimori, J. Watanabe, M. Shoji, and A. Nagai, *Jpn. J. Appl. Phys.* **27**, L2351 (1988).
84. M. Naoe, N. Kitamura, M. Shoji, and A. Nagai, *J. Appl. Phys.* **63**, 3636 (1988).
85. K. Takanashi, J. Watanabe, G. Kido, and H. Fujimori, *Jpn. J. Appl. Phys.* **29**, L306 (1990).
86. K. Takanashi, K. Sato, J. Watanabe, Y. Sato, and H. Fujimori, *Jpn. J. Appl. Phys.* **30**, 52 (1991).
87. K. Sato, H. Ikekame, H. Hongu, M. Fujisawa, K. Takanshi, and H. Fujimori, in: *Proc. of the Sixth Int. Conf. on Ferrites*, (Jpn. Society of Powder and Powder Metallurgy, Tokyo) (1992), p. 1647.
88. H. Ikekame, K. Sato, K. Takanashi, and H. Fujimori, *Jpn. J. Appl. Phys.* **32**, *Suppl.* 32-3, 284 (1993).
89. P. A. M. van der Heide, W. Baelde, R. A. de Groot, A. R. de Vroomen, P. G. van Engen, and K. H. J. Buschow, *J. Phys. F: Metal Phys.* **15**, L75 (1985).
90. G. Q. Di, S. Iwata, S. Tsunashima, and S. Uchiyama, *J. Magn. Soc. Jpn.* **16**, 113 (1992).
91. G. Q. Di, *Ph.D. Thesis*, Nagoya University (1992).
92. C. H. Shang, Z. H. Guo, Y. Xu, and Y. J. Wang, in: *Proc. Third Int. Conf. on Phys. of Magn. Mater.* (Seoul, Korea, (1995), p. 515.
93. G. Q. Di, S. Iwata, S. Tsunashima, and S. Uchiyama, *J. Magn. Magn. Mater.* **104-107**, 1023 (1992); G. Q. Di, S. Iwata, and S. Uchiyama, *ibid.* **131**, 242 (1994).
94. Tu Chen and W. E. Stutius, *IEEE Trans. Magn. MAG* **10**, 581 (1974).
95. P. Villars and L. D. Calvert, *Pearson's Handbook of Crystallographic Data for Intermetallic Phases*, ASM International, Materials Park (1991).
96. R. Pittini, J. Schoenes, O. Vogt, and P. Wachter, *Phys. Rev. Lett.* **77**, 944 (1996).
97. R. Pittini, J. Schoenes, and P. Wachter, *Phys. Rev.* **B55**, 7524 (1997).
98. R. Pittini, J. Schoenes, and P. Wachter, *Physica* **B206-207**, 92 (1995).

99. A. J. Freeman and D. D. Koelling, *The Actinides: Electronic Structure and Related Properties*, A. J. Freeman and J. E. Darby (eds.), Academic Press, New York (1974), Vol. 1; E. Warren, E. Picket, A. J. Freeman, and D. D Koelling, *Phys. Rev.* **B22**, 2965 (1980).
100. B. Johansson, *Phys. Rev.* **B11**, 2740 (1975).
101. H. I. Skriver, O. K. Andersen, and B. Johansson, *Phys. Rev. Lett.* **41**, 42 (1978); *ibid.* **44**, 1230 (1980).
102. M. S. S. Brooks, *J. Magn. Mater.* **29**, 257 (1982); *J. Phys.* **F13**, 103 (1983).
103. *Handbook of Physics and Chemistry of the Actinides*, A. J. Freeman and G. H. Lander (eds.), North-Holland, Amsterdam (1984).
104. J. Friedel, *J. Phys. Chem. Solids* **1**, 175 (1956).
105. R. C. Albers, A. M. Boring, J. M. Wills, L. E. Cox, O. E. Eriksson, and N. E. Christensen, *Phys. Rev.* **B54**, 14405 (1996).
106. V. N. Antonov, A. I. Bagljuk, A. Ya. Perlov, V. V. Nemoshkalenko, Vl. N. Antonov, 0. K. Andersen, and O. Jepsen, *Low Temp. Phys.* **19**, 792 (1993).
107. T. Gasche, M. S. S. Brooks, and B. Johansson, *Phys. Rev.* **B54**, 2446 (1996).
108. J. Kollar, L. Vitos, and H. L. Skriver, *Phys. Rev.* **B55**, 15353 (1997).
109. P. Sderlind, J. M. Wills, B. Johansson, and O. Eriksson, *Phys. Rev.* **B55**, 1997 (1997).
110. J. van Ek, P. A. Sterne, and A. Gonis, *Phys. Rev.* **B48**, 16 280 (1993).
111. J. D. Becker, J. M. Wills, L. Cox, and B. R. Cooper, *Phys. Rev.* **B54**, 17265R (1996).
112. L. M. Sandratskii and J. Kübler, *Phys. Rev.* **B55**, 11395 (1997).
113. H. Kumigashira, S.-H. Yang, T. Yokoya, A. Chaiani, T. Takahashi, A. Uesawa, T. Suzuki, O. Sakai, and Y. Kaneta, *Phys. Rev.* **B54**, 9341 (1996).
114. D. A. Bonn, J. D. Garrett, and T. Timusk, *Phys. Rev. Lett.* **61**, 1305 (1988).
115. L. Degiorgi, M. Dressel, G. Griiner, N. Sato, and T. Komatsubara, *Europhys. Lett.* **25**, 311 (1994).
116. P. Wachter, in: *Handbook on the Physics and Chemistry of the Rare Earths*, K. A. Gschneidner, Jr., L. Eyring, G. H. Lander, and G. R. Choppin (eds.), North-Holland, Amsterdam (1994), Vol. 19, p. 177.
117. W. Reim, *J. Magn. Magn. Mater.* **58**, 1 (1986).
118. F. Hulliger, *J. Less-Comm. Metals* **16**, 113 (1968).
119. J. Leciejewicz and A. Zygmunt, *Phys. Status Solidi* **A13**, 657 (1972).
120. A. Zygmunt and M. Duczmal, *Phys. Status Solidi* **A9**, 659 (1972). K. P. Belov, A. S. Dmitrievsky, A. Zygmunt, R. Z. Levitin, and V. Trzebiatowski, *Zh. Eksp. Teor. Fiz.* **64**, 582 (1973).
121. J. Brunner, M. Erbudak, and F. Hulliger, *Solid State Commun.* **38**, 841 (1981).
122. A. Blaise, R. Lagnier, A. Wojakowski, A. Zygmunt, and M. J. Mortimer, *J. Low Temp. Phys.* **41**, 61 (1980).
123. V. Sechovsky and L. Havela, in: *Ferromagnetic Materials*, E. P. Wohlfarth, and K. H. J. Buschow (eds.), North-Holland, Amsterdam (1988), Vol. 4, p. 309. L. M. Sandratskii and J. Kiibler, *Solid State Commun.* **91**, 183 (1994).
124. A. Hiess, L. Havela, K. Prokes, R. S. Eccleston, and G. H. Lander, *Physica* **B230-232**, 89 (1997).
125. K. A. McEwen, U. Steigenberger, and J. L. Martinez, *Physica* **B186-188**, 670 (1993).
126. J. A. Paixao, G. H. Lander, P. J. Brown, H. Nakotte, F. R. de Boer, and E. Brück, *J. Phys.: Condens. Matter.* **4**, 829 (1992).
127. J. A. Paixao, G. H. Lander, A. Delapalme, H. Nakotte, F. R. de Boer, and E. Brück, *Europhys. Lett.* **24**, 607 (1993).
128. P. A. Veenhuizen, F. R. de Boer, V. Menovsky, V. Sechovsky, and L. Havela, *J. Appl. Phys.* **63**, 3064 (1988).
129. P. Beránková, M. Kucera, M. Matyás, and A. A. Menovsky, in: 26^{iemes} *Journées des Actinides*, Szklarska Poreba, Poland, (1996), p. 70.
130. J.-M. Fournier and R. Troc, in: *Handbook on the Physics and Chemistry of the Actinides*, A. J. Freeman, and G. H. Lander (eds.), North-Holland, Amsterdam (1985), Vol. 2, p. 29.
131. D. L. Tillwick and P. de V. du Plessis, *J. Magn. Magn. Mater.* **3**, 329 (1976).
132. G. Busch, O. Vogt, A. Delpalme, and G. H. Lander, *J. Phys.* **C12**, 1391 (1979).
133. G. H. Lander, M. S. S. Brooks, B. Lebech, P. J. Brown, O. Vogt, and K. Mattenberger, *J. Appl. Phys.* **69**, 4803 (1991).
134. M. S. S. Brooks and P. J. Kelly, *Phys. Rev. Lett.* **51** (1983)
135. G. H. Lander, *Physica* **B186-188**, 664 (1993).
136. M. M. S. Brooks, *Physica* **B130**, 6 (1985).
137. J. Schoenes, B. Frick, and O. Volt, *Phys. Rev.* **B30**, 6578 (1984).
138. J. Schoenes, *Physica* **B102**, 45 (1980).
139. J. Schoenes, in: *Handbook on the Physics and Chemistry of the Actinides*, A. J. Freeman, and CD. H. Lander (eds.) North-Holland, Amsterdam (1984), Vol. 1, p. 341.
140. B. R. Cooper, Q. G. Sheng, S. P. Lim, C. Sanchez-Castro, N. Kioussis, and J. M. Wills, *J. Magn. Magn. Mater.* **108**, 10 (1992).
141. M. S. S. Brooks, T. Gasche, and B. Johansson, *J. Phys. Chem. Solids* **56**, 1491 (1995).
142. B. Reihl, N. Martensson, and O. Vogt, *J. Appl. Phys.* **53**, 2008 (1982).
143. L. Severin, M. S. S. Brooks, and B. Johansson, *Phys. Rev. Lett.* **B71**, 3214 (1993).
144. J. Köhler, L. M. Sandratskii, and J. Kuber, *Phys. Rev.* **B55**, 10153R (1997).
145. V. N. Antonov, V. P. Antropov, B. N. Harmon, A. N. Yaresko, and A. Ya. Perlov, submitted to *Phys. Rev.* **B**. (1999).